UPPSALA
UNIVERSITET

UU-NF 06#02
(February 2006)
Uppsala University Neutron Physics Report
ISSN 1401-6269

Study of the pulse shape as a means to identify neutrons and gammas in a NE213 detector

MIKAEL HÖÖK

DIPLOMA THESIS

UPPSALA UNIVERSITY
DEPARTMENT OF NEUTRON RESEARCH
PROGRAM OF NEUTRON PHYSICS
UPPSALA, SWEDEN

UPPSALA
UNIVERSITET

UU-NF 06#02 (March 2006)
UPPSALA UNIVERSITY NEUTRON PHYSICS REPORT
ISSN 1401-6269
Editor: J Källne

Study of the pulse shape as a means to identify neutrons and gammas in a NE213 detector

Mikael Höök

Department of Neutron Research, Uppsala University,
BOX 525, SE-75120 Uppsala, Sweden

Abstract

This report describes investigations of the NE213-detector and the possibility to utilize pulse shape analysis to separate neutrons and gammas in a mixed emission field. Neutron fluxes are often contaminated with gammas, to which the detectors are sensitive. Sorting out the unwanted gamma pulses from the interesting neutrons is therefore crucial in many situations, for instance in fusion reactor diagnostics, such as for neutron cameras. This can be done based on pulse shapes, which differ for gammas and neutrons interacting in the NE213-detector. By analyzing the pulse shapes from a digital transient recorder, neutrons can be distinguished from gammas. An experiment with a Cf-252 neutron source was set up and provided data. The separation algorithm was based on charge comparison and gave good results. Furthermore the results of the pulse shape analysis were verified by TOF-measurements. The lowest permissible energy for a reasonable separation was found to be around 0.5 MeV. Some conclusions on the limitations of the equipment were also made.

UPPSALA UNIVERSITY
DEPARTMENT OF NEUTRON RESEARCH
PROGRAM OF NEUTRON PHYSICS
UPPSALA, SWEDEN

Table of contents

1. Introduction

Liquid scintillators such as NE213 are cheap and reliable and are a part of the diagnostics of fusion reactors. Today they are used to measure radiation fluxes in neutron cameras, but later on they will probably be an integrated part of a larger and more complex detector system.

One major problem is that the neutron flux has an admittance of gamma rays to which the detectors are sensitive. A good way of separating the neutrons from the gammas must therefore be found. This can be afforded by means of pulse shape of gamma and neutron signals from a NE213 liquid scintillator, which is different.

The advantage of using a fast digitization technique to store the pulses offers high-count rate operation, pulse shape analysis possibilities, post-experiment data re-processing and pile-up treatment and identification.

NE213 scintillators have already been used successfully for measurements in mixed neutron and gamma radiation fields from fusion plasmas [1], [2] and for separation of alpha- and beta-radiation [3]. Separation between gammas and neutrons can be done by software comparison of the pulse charge in different time intervals and count rates in the MHz range has been achieved.

The purpose of this thesis is to study the possibilities to use pulse shape analysis and a NE213 detector to separate gammas and neutrons. By looking at existing data and setting up a new experiment a useful method for separation will be found. The possibilities of pulse shape discrimination will also be investigated.

2. Background

A brief overview of the most important parts of the physics behind gamma and neutron detection, scintillators and pulse shape analysis (PSA) is needed to fully grasp the content of this thesis.

2.1 Gamma detection

Gammas are uncharged and create no direct ionization or excitation when it passes though a material. The detection is therefore critically dependant on gamma-ray interactions that transfer all or part of its energy to an electron. The electron subsequently deposits its energy in the scintillator, giving rise to a light pulse, which is proportional to the energy. These interactions can be Compton scattering, pair production or photoelectric, of which the first type is dominating in this case.

In a liquid scintillator gammas primary knock off electrons. The recoil electrons from Compton scattering form a continuum, ranging from zero to the maximum energy that can be transferred from the gamma. Photo peaks from certain gamma energies can also be seen, but are very weak and negligible.

2.2 Neutron detection

To be able to detect a neutron one must transfer its energy to a charged particle. There are several ways to make this energy transfer but the simplest is elastic scattering on light nuclei. The advantage of using light nuclei, such as hydrogen, is that the entire neutron energy can be transferred at once, while a heavy nucleus only can accept a small faction of the neutron energy.

2.2.1 Elastic scattering

Nuclear scattering includes collisions between a nucleon and a nucleus or two nuclei in which kinetic energy can be transferred from one to the other. Specified if an incoming nucleon collides with a stationary target nucleon or nucleus, a recoil nucleon is created with certain energy. Hydrogen, deuterium or helium is a useful target for elastic scattering of neutrons, but hydrogen is the most interesting since it is the lightest of them. The recoil nuclei generated by elastic neutron scattering on hydrogen is called recoil protons [4].

By definition the total kinetic energy is the same both before and after elastic scattering, i.e. collision with zero Q-value. The target nucleus is in rest and that makes the sum of the kinetic energy for the scattered neutron and the recoil nucleus to be the same as the kinetic energy of the incoming neutron. The lowest neutron energy that can be measured is limited by the lowest kinetic energy of the recoil nucleus that the detector can determine.

In hydrogen it is possible for the incoming neutron to transfer everything from zero to its full energy to the target nucleus. This makes the mean energy of the recoil proton to be about half the initial neutron energy.

One can detect fast neutrons in the presence of gamma rays or similar low energetic background, but the distinction will be harder and harder when the energy of the incoming neutron becomes lower and lower. Despite this fact is it possible to identify sub MeV-neutrons by using special proton recoil detectors that utilize pulse shape discrimination techniques.

The elastic nucleon-nuclei collision is determined by two-body mechanics, which is described below with the following terminology. The scattering in both the lab system and the center-of-mass system is described in figure 1.

A = Mass of the target nucleus
E_n = Kinetic energy of the incoming neutron (lab-system)
E_r = Kinetic energy of the recoil nucleus (lab-system)
Θ = Scattering angle of the neutron in center-of-mass coordinate system
θ = Scattering angle of the recoil nucleus in the lab-system

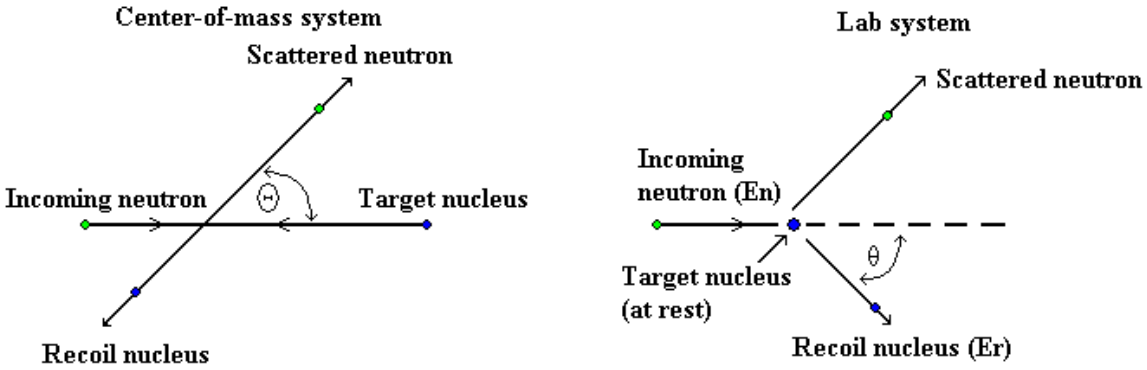

Figure 1: Scattering in the lab system and the center-of-mass system

For the non-relativistic case ($E_n << 939$ MeV) one can derive the following equation for the recoil nucleus by using the conservation of momentum and energy in the center-of-mass coordinate system.

$$E_r = \frac{2A}{(1+A)^2}(1-\cos\Theta)E_n \qquad (2.1)$$

The transformation between the angles is done by the following formula:

$$\cos\theta = \sqrt{\frac{1-\cos\Theta}{2}} \qquad (2.2)$$

Combining 2.1 and 2.2 one gets the following equation for the recoil nucleus energy

$$E_r = \frac{4A}{(1+A)^2}(\cos\theta)^2 E_n \qquad (2.3)$$

The energy of the recoil nucleus is determined by the angle of scattering. The maximum takes place when the cos θ equals zero, when θ is 0 degrees. The resulting maximum energy becomes:

$$E_{r\max} = \frac{4A \cdot E_n}{(1+A)^2} \qquad (2.4)$$

The neutron can only transfer the entire energy to the recoil nucleus if the mass of the recoil nucleus, A, is 1. One can therefore see why hydrogen and other light nuclei are so dominating for neutron detection. A heavy nucleus can only accept a small fraction of the neutrons energy and that makes them kind of unsuitable for detectors, but very useful in for instance fast neutron reactors where light nuclei would slow down the neutrons too much. The maximum amount of energy that can be transferred for some different nuclei can be seen in table 1.

Target nucleus	A	Maximum $E_r/E_n = 4A/(1+A)^2$
H-1	1	1
H-2	2	8/9 ≈ 0.888889
He-3	3	3/4 = 0.75
C-12	12	48/169 ≈ 0.284023
O-16	16	64/289 ≈ 0.221453
Fe-56	56	224/3249 ≈ 0.06894
Pb-208	208	832/47961 ≈ 0.01734

Table 1: Maximum energy transferred by the neutron for different nuclei

It is not only the maximum energy that can be transferred to the recoil nuclei. The transferred energy will be distributed between the minimum of zero and the maximum given by formula (2.4). The transferred energy will be a continuum between the two extremes.

The differential scattering cross section is defined as σ(Θ) in the center-of-mass system. This leads to that the probability of a neutron to be scattered into dΘ about

Θ will become the following where σ_s is the total scattering cross section integrated over all angles:

$$P(\Theta)d\Theta = 2\pi \sin\Theta d\Theta \frac{\sigma(\Theta)}{\sigma_s} \qquad (2.5)$$

It is more interesting to see the distribution in recoil nucleus energy. If one allow $P(E_r)dE_r$ be the probability of creating a recoil nucleus with energy dE_r about E_r one can obtain the following since $P(E_r)dE_r = P(\Theta)\, d\Theta$:

$$P(E_r) = 2\pi \sin\Theta d\Theta \frac{\sigma(\Theta)d\Theta}{\sigma_s dE_r} \qquad (2.6)$$

Evaluating $d\Theta/dE_r$ from equation (2.1) and substituting one obtains:

$$P(E_r) = \frac{\pi(1+A)^2}{A * E_n * \sigma_s}\sigma(\Theta) \qquad (2.7)$$

Equation (2.7) implies that the recoil energy continuum is shaped like the differential cross section, $\sigma(\Theta)$, as a function of the center-of-mass scattering angle. The structure of $\sigma(\Theta)$ will be peaked to favor forward or backward scattering, at least for most target nuclei. If the scattering is isotropic in the center-of-mass-coordinate system a very important simplification can be done. This makes the $\sigma(\Theta)$ invariant with Θ and is equal to a constant $\sigma_s/4\pi$. This astonishing case is not generally true, but it holds for scattering from hydrogen over most of the energy range $E_n < 10$ MeV. Since hydrogen is the most important target for neutron studies, this remarkable simplification is of major importance. The response function of a detector based on hydrogen scattering should thus be of simple rectangular shape. The average recoil proton energy is then half of the neutron energy. However the rectangular response is distorted by a number of complicating factors.

Proton recoil scintillators

The NE213 detector is hydrogen rich and that makes it suitable for detecting neutrons. The fast neutrons create recoil protons that can be transformed into electric signals by the photomultiplier tube. The transferred energy from the neutrons to the recoil protons is approximately rectangular ranging from zero to the maximum transferable energy. Since the range of the recoil protons are much shorter than the size of the detector, the full energy of the protons will be deposited inside the detector and the expected pulse height distribution is therefore also roughly rectangular.

2.2.2 Time-of-flight method (TOF)

The time-of-flight method is probably the most common when it comes to fast neutron spectroscopy. It utilizes fast and exact time measurements and the electronics for that kind of purpose is commercially available. This makes TOF-measurements both cheap and useful. The simplicity is also a big advantage. If one knows the time of flight for a certain length it is possible to calculate the kinetic energy of the neutron from basic relations.

m_0 = rest mass of the neutron [939.5656 MeV/c^2]
m = mass of the neutron [MeV/c^2]
c = 2.99792*10^8 [m/s]
E_n = kinetic energy of the neutron [MeV]
s_n = length of flight [m]
t_n = time of flight for the neutron [s]
v_n = velocity of the neutron [m/s], ($v_n = s_n/t_n$)

The kinetic energy is obtained from the following formula:

$E_n = mc^2 - m_0c^2$ where $m = \frac{m_0}{\sqrt{1-(v_n/c)^2}}$ (2.8)

Which gives the following relation

$$E_n = \frac{m_0c^2}{1-\sqrt{(\frac{s_n}{t_n * c})^2}} - 1 \quad (2.9)$$

A drawback with TOF-measurements exists for low energy neutrons. Because of the low neutron energy there is a significant difference in velocity between the neutrons and the scintillation light. Depending on where in the detector the neutron interacts it will get a difference in time of flight. For instance, a neutron with energy of 5 MeV will have a velocity of 31 mm/ns while light travels in 200 mm/ns in NE213. The time it takes for a 5 MeV neutron and a photon to travel though a 10 cm thick detector is 3.2 ns respectively 0.5 ns. This means that the time of flight can differ up to 2.7 ns for a 5 MeV neutron depending on where in the detector it interact. This can be a problem for accurate measurements of low energy neutrons, but can often by avoided.

2.2 Scintillation detectors

The scintillator principle for detection of radiation is one of the oldest ways to distinguish radiation known to man. The phosphorescing screens used by scientists like Wilhelm Röntgen, Hans Geiger and Ernest Rutherford were the first real time detectors and a first version of the scintillators used today.

A scintillator transforms the energy of the particle to light that can be detected, ideally with high efficiency. Other desired properties are linearity, transparence for the emitted light, and short decay time for the induced luminescence so high pulse rate can be obtained together with good optical properties. No material possesses all these characteristics so scintillators are often a compromise between the factors above and a few more.

A large amount of different types of scintillators exists. Each kind has its advantages and drawbacks. The inorganic scintillators have the best light output but suffer from slow response time. Organic counterparts have lower light output but they are very fast. The application is of great importance for which type of scintillator one should use. Inorganic crystals are often used for gamma detection while organic ones are suitable for neutron detection.

The scintillation mechanism in organics:
In an organic scintillator the scintillation mechanism comes from transitions in the energy levels for the molecules. Many commercially available detectors are based on organic molecules with specific symmetry properties.

The electron structure can be separated into singlet (S_0, S_1, S_2, …) and triplet states (T_1, T_2, T_3, …). The molecules used for detectors have an energy gap between S_0 and S_1 of about 3-4 eV and thereafter decreasing energy gaps between higher energy levels. These levels can be expanded into more sublevels called vibrational states with a much finer structure.

Typical energy gaps between vibrational states are about 0.15 eV. To distinguish different states from each other a second index is introduced. S_{00} denotes the lowest vibrational state in the lowest electronic state. Since the energy difference between the ground state and the lowest vibrational state is much higher than the average thermal energy of around 0.025 eV, nearly all electrons will be in the S_{00}-state.

By absorbing kinetic energy from a charged particle that passes nearby, electrons can be excited to higher states. Higher electronic singlet states are quickly de-excited to the S1 electron state via radiationless internal conversion, which happens in a few picoseconds. States with higher vibrational energy is not in thermal equilibrium with neighboring molecules and quickly loses its excess energy. The total net effect of an excitation process in an organic compound is that after a short time a population of excited molecules in the S_{10} state is produced.

The fast light or prompt fluorescence is emitted from transitions between the S_{10} state and vibrational states in the S_0 electronic ground state. In most organic scintillators the decay constant of the prompt fluorescence is about a few nanoseconds and therefore the prompt scintillation component is relatively fast.

The delayed fluorescence comes from decay of triplet states. Though a process called intersystem crossing some excited singlet states can be converted into triplets. The lifetime for a triplet state T_1 is much longer than for a singlet state. The lifetime may be as long as 10^{-3} seconds and the de-excitation of the triplet states will be a delayed light emission known as delayed fluorescence of slow light. See figure 3 for a graphic display of the level scheme and transitions.

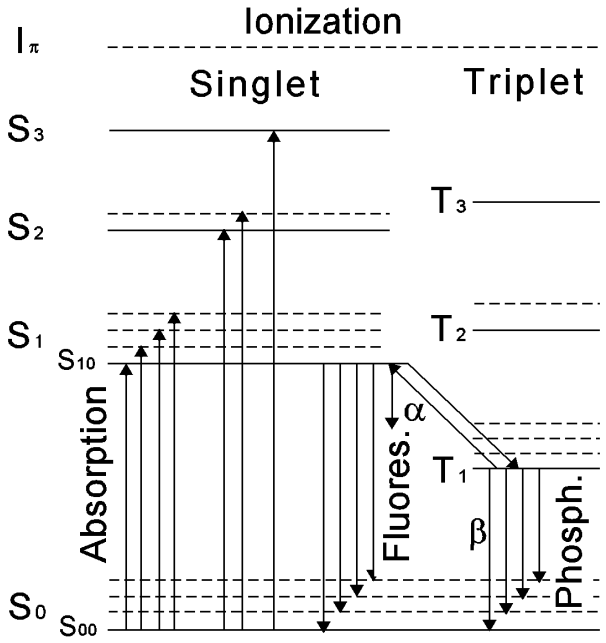

Figure 3: Transition scheme for the excitations and de-excitations in an organic scintillator. Phosphorescence is another word for delayed fluorescence

Efficiency and quenching:

Scintillators are usually transparent to their own fluorescent emission. There is a very little overlap between the absorption and emission spectra and therefore very little self-absorption of the fluorescence light.

The scintillator efficiency is defined as the amount of incident particle energy that is converted into light. Since there exist a number of alternative de-excitation processes that do not emit light, unfortunately all the absorbed particle energy will not be transformed to light. All such radiationless de-excitation processes are grouped together under the term "quenching". To make it as small as possible it is important to eliminate impurities that may degrade the light output [4].

Liquid scintillators:

Organic compounds can easily be mixed with a suitable solvent and thus creating a liquid scintillator. An advantage of liquid scintillators is that they lack a solid structure and thereby becomes more resistant against radiation damage compared to solid of plastic scintillators. Another advantage is that they often are cheap compared to other detectors.

Response functions:

Light response: A part of the kinetic energy of a charged particle inside the scintillator is converted into fluorescent energy. The rest is dissipated as heat or by other non-radiatively processes. How much of the particle energy that is converted depends on both the particle type and its energy.

Several commercially available scintillators have a linear response to electrons with energies higher than about 125 keV. Heavier charged particles like alphas or protons have nonlinear behavior to much higher initial energies and lower response than for electrons. At energies of a few hundred keV, the response to protons is smaller by a factor of 10 compared with the light yield of equivalent energy electrons [4]. At higher energies the dissimilarity is less, but the proton response is always below the electron response. More exact relations for the proton response can be found under the chapter 'NE213 characteristics'.

Time response: One can assume that the luminescent states in an organic molecule are formed instantaneous and only prompt fluorescence is observed. This reduces the time profile of the light pulse to a very fast leading edge with a simple exponential decay as a tail.

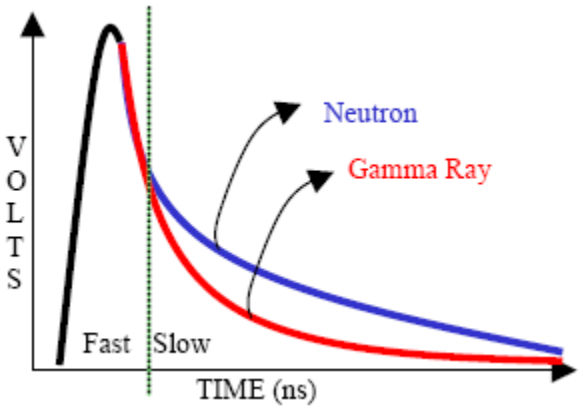

Figure 4: The difference between gammas and neutrons in an organic scintillator pulse

This uncomplicated representation of the pulse is often enough to describe many phenomena of the scintillator behavior, but sometimes a more detailed description is needed. By also taking the finite time required to populate the luminescent states and the slower components of the scintillation into account one obtains a more accurate picture [5].

When a neutron enters the liquid of the scintillator it will interact with it by hitting a proton of the hydrogen nucleus, while a gamma Compton scatter off an electron. The scattered particle will excite the surrounding molecules and create emission of light that later can be picked up by a photo multiplication tube and transformed into an electric signal. Figure 4 shows the difference. Figure 5 and 6 shows some measured differences.

The pulse that comes from the PM-tube is a sum of two exponential decays. The first one is the fast part that comes from the initial interactions that occurs in the scintillator. It has a high decay constant and falls of quickly, hence the name fast signal.

The second part comes from the secondary interactions that occur when the charged particle collides with other particles. It is a smaller signal than the first one, but it has a longer lifetime. This is called the slow signal.

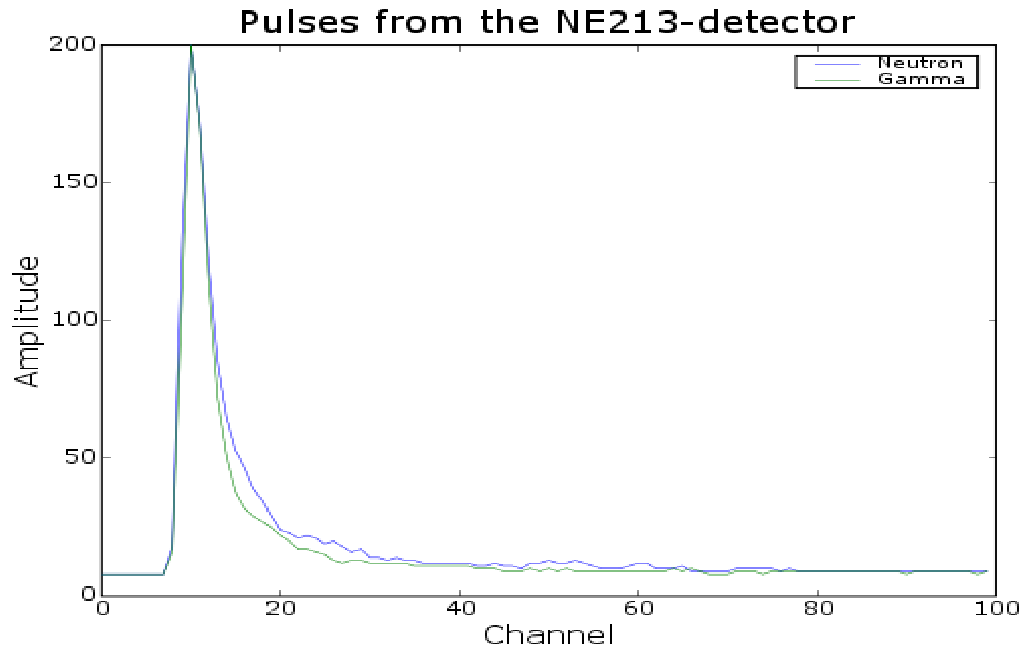

Figure 5: Gamma induced and neutron induced pulses measured with the NE213-detector. The small difference in the tails can be seen.

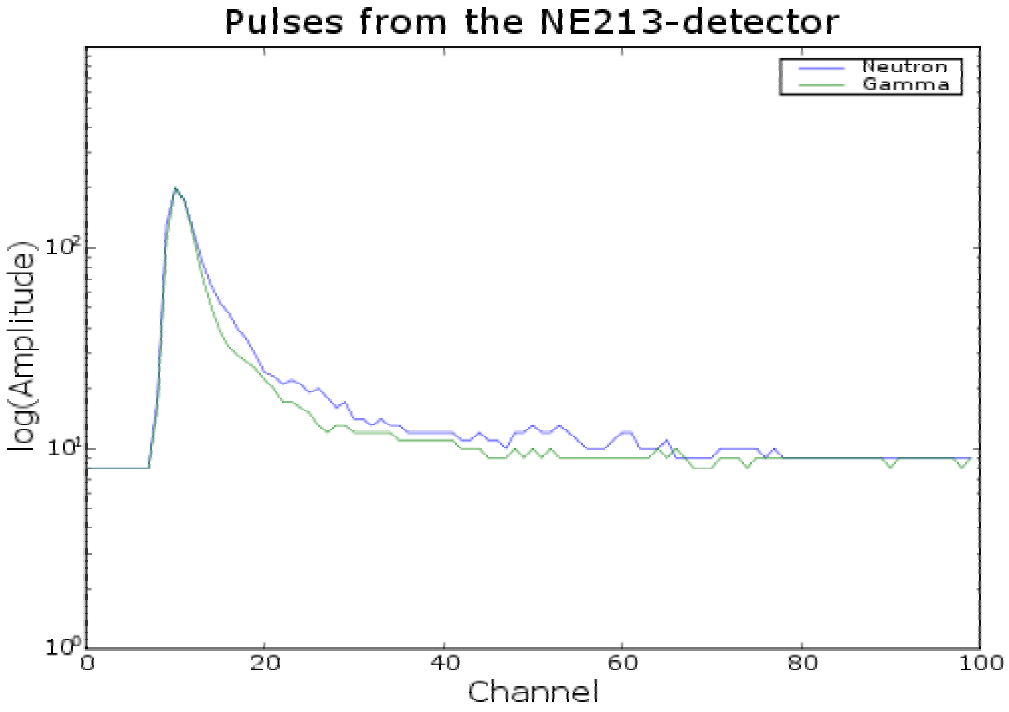

Figure 6: A lin-log plot of the same pulses more clearly displays the difference

2.2.1 NE213 Characteristics

The NE213 detector is an organic scintillator with several useful properties. It has fast time response. Ionizing particles produced light pulses that can be classified as either electron-like or proton-like. A proton-like pulse has a relatively more exaggerated tail due to long-lived scintillation components. An electron-like pulse has a smaller tail since it lacks the long-lived components of the proton interactions. These two cases of pulse shapes are useful for separating the different kind of radiations that caused them. Figure 7 shows the detector.

NE213 properties:

Light Output (% Anthracene)	78%
Wavelength of Maximum Emission	425 nm
Atomic Ratio, H:C	1.212
No. of C Atoms per cm^3	$3.98*10^{22}$
No. of H Atoms per cm^3	$4.82*10^{22}$
No. of Electrons per cm^3	$2.27*10^{23}$
Refractive Index	1.505
Decay Time (short component)	3.2 ns
Mean Decay Times of First 3 Components	3.16, 32.3 & 270 ns

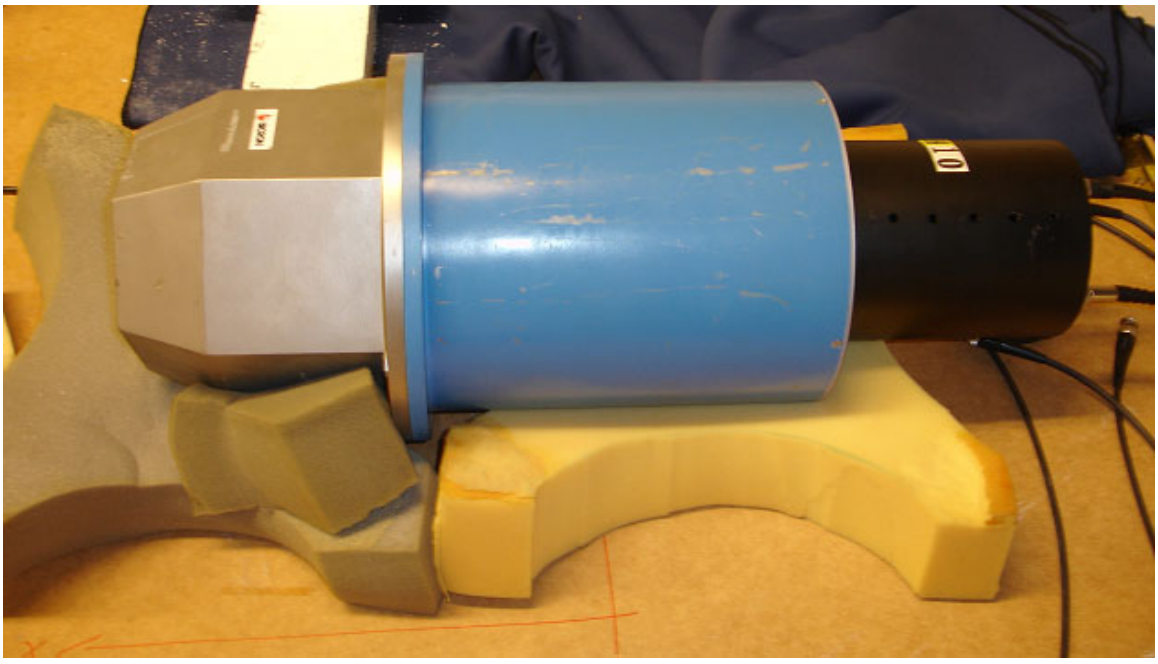

Figure 7: The NE213 detector used in the experiments. The grey part is the shell containing the liquid scintillator and the blue/black cylinder is the PM-tube

Response to Protons:
A recoil proton interacting inside the NE213-detector will produce less light than an electron of equivalent kinetic energy. When an electron and a neutron generate the same amount of light it is called electron equivalent kinetic energy (MeV_{ee}), see figure 8 for a graphic display of the relation. For a NE213 detector this relation has the following form:

$$E = 0.83P - 2.82*(1-\exp(-0.25*P^{0.93})) \qquad (2.10)$$

Where P is the proton energy in MeV and E is the electron energy in MeV that gives the same light output in the range 1-300 MeV [6]. A more precise study in the energy range of 5-17 MeV developed a more accurate relationship [7].

An alternative relationship valid in the energy range of 0 to 75 MeV can be found in reference [8] and looks like:

$$E = -10.7*(1-\exp(-0.07*P^{0.89}))+0.93*P \qquad (2.11)$$

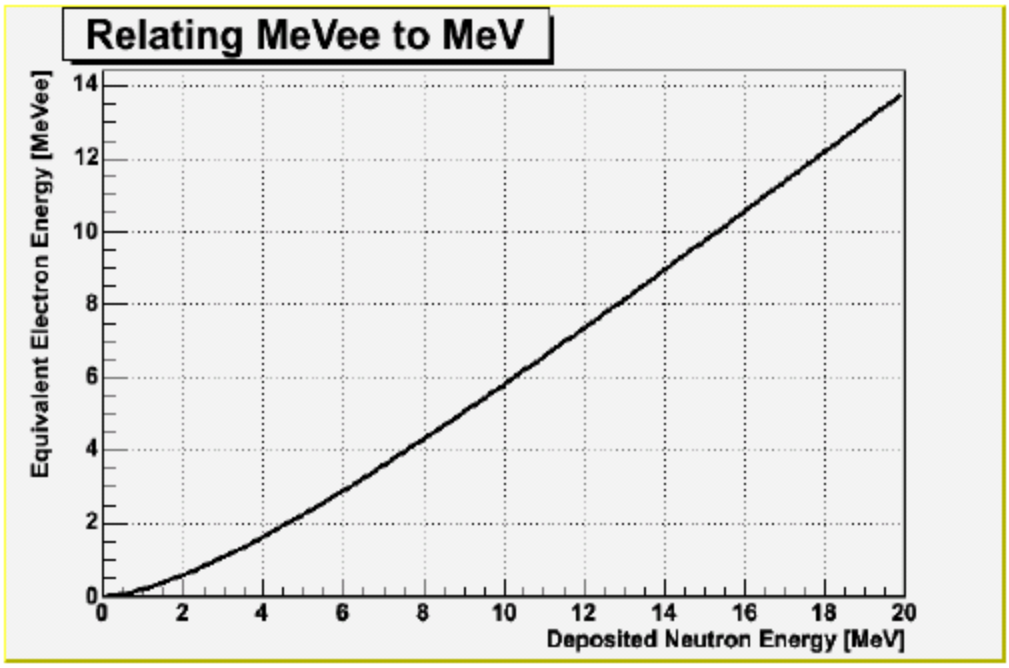

Figure 8: The relation between MeV and MeV_{ee}

2.3 Radioactive sources

Many different materials and isotopes have radioactive properties. Some of the nuclides have suitable properties for calibration and tests of scintillation detectors.

2.4.1 Na-22

Man has known sodium[1] since the time of the ancient Greeks and the radioactive isotope Na-22 with half-life of 2.6 years. The decay is positron emission with a maximum energy of 0.545 MeV. Accompanying gammas of 1.275 MeV and annihilation gammas of 0.511 MeV are also seen. The Na-22 sample was used in the present study for the purpose of energy calibration and for obtaining pure spectra of gammas without any neutrons. The pulse height spectrum can be seen in figure 9.

The source used had an activity of 15-20 μCi making it an A-classed sample with low hazard.

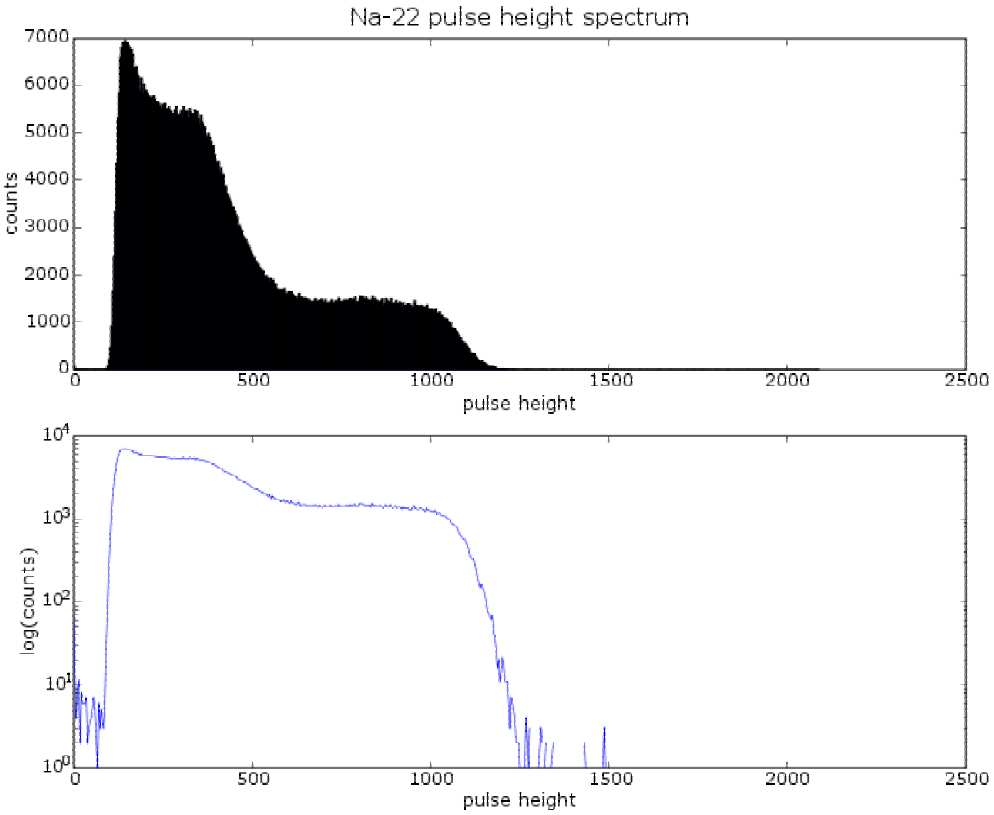

Figure 9: Pulse height spectra obtained for Na-22

[1] The name Na derives from the Latin word "natron" meaning "impure salt". The English name sodium comes from "soda" since sodium was purified from the electrolysis of caustic soda.

2.4.2 Cf-252

Thompson, Seaborg, Street and Ghioirso discovered Californium in the year of 1950 by bombarding small quantities of Cm-242 with 35 MeV helium ions from a cyclotron. It is the sixth transuranium element and has different uses in industry due to its useful properties. Cf-251 is of military interest because of the exceptionally small critical mass for nuclear fission.

The isotope Cf-252 is a very strong neutron source due to remarkably high spontaneous fission rate. One microgram releases 170 million neutrons per minute. The isotope has already found use in neutron moisture gauges used in the determination of water and oil-bearing layers. It is also used as a portable neutron source for localization of metals like gold and on-the-spot neutron activation analysis.

Cf-252 has a half-life of 2.645 years. The decay is branched into 3.1% spontaneous fission and 96.9% alpha decay. The main part of the energy spectrum of the neutrons is peaked around 0.8 MeV although some neutrons have as high energies as 8 or 10 MeV. Figure 10 shows the neutron energy distribution.

The Cf-252 sample that was used had an activity of 16 μCi and was therefore an A-classed sample with low hazard.

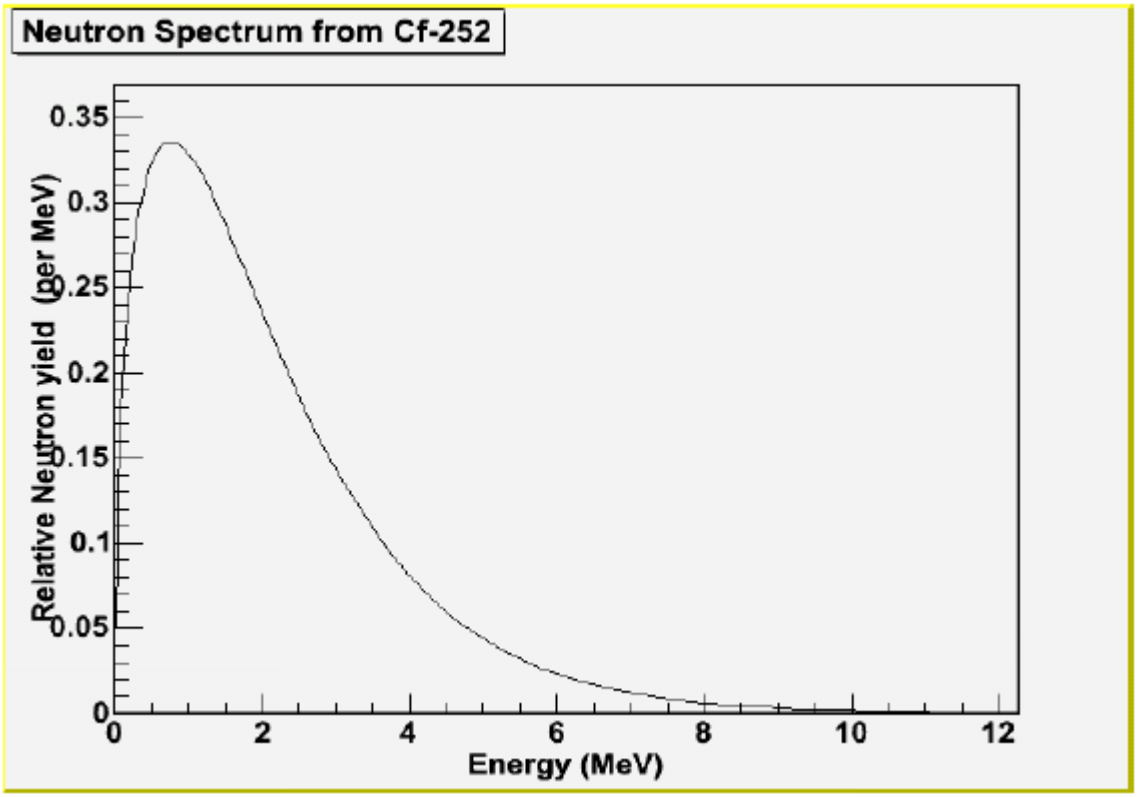

Figure 10: The energy distribution of neutrons from Cf-252. The peak is around 1 MeV of neutron energy. [IAEA]

2.4.3 Background radiation

During the experiment some background radiation was present. This was mostly cosmic muons besides gammas from K-40 and other common gamma emitters. Since the NE213 detector was big a cosmic muon could deposit energy up to over 1 MeV. Quite many gamma rays emitted from mostly K-40 could also be seen. The pulse height spectrum can be seen in figure 11.

Luckily the vast majority of cosmic background interactions cause electron-like pulses and can therefore quite clearly be distinguished from the proton-like interactions of the neutrons.

In order to reduce the background several blocks of lead were placed around the detector, however due to limited amount of lead and the difficulty to stop muons some background could still be seen among the measured pulses.

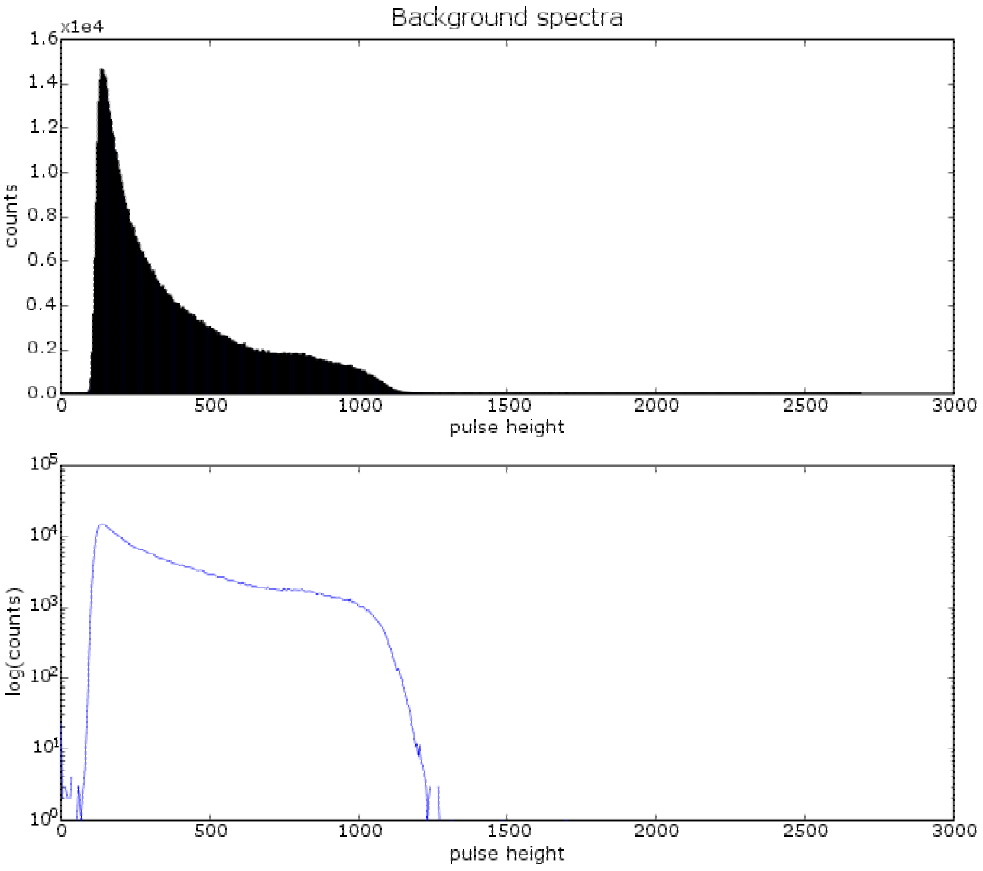

Figure 11: Pulse height spectra obtained for the background radiation. The small bump around pulse height 800 comes from K-40

3. Setup and measurements

An experiment was setup to get new data. The idea was to include a time-of-flight measurement to verify the separation of signals based on the pulse shapes.

The neutron emission of Cf-252 was accompanied by prompt gammas and therefore a coincidence technique could be used. This allowed one to distinguish between gamma-gamma and gamma-neutron pairs by measuring the time difference between them. The difference in flight time between neutrons and gammas is quite large and a clear distinction can therefore be made. The results from the TOF-measurements could hence be used to verify the pulse shape analysis (PSA).

3.1 Experimental setup

A distance of around 60 cm separated two detectors. The smaller detector was a barium fluoride crystal coupled with a PM-tube. The big detector was the NE213-scintillator with PM-tube. Figure 12 shows a picture of the setup.

Figure 12: The TOF-setup. The blue/grey item is the big NE213 detector while the smaller BaF-detector and the radioactive sample can be found behind the white lead blocks.

3.2 Electronics and equipment

A four-channel 200-MHz digital transient recorder card (TR) was used in the experiment. The card was used to record pulse shapes with 8-bit resolution and could only handle pulses between –1 and 0 Volts in amplitude. Smaller pulses was truncated at –1 Volt and this caused some corrupted pulses which were discarded.

The card had the ability of operating with open acquisition. This means that the card recorded the pulse before the trigger. The internal memory of the card was 512 Mb which corresponds to between 500 000 to 2 million pulses depending on desired pulse size.

A time-to-pulse height converter of type Ortec model 437 was used together with a Constant-Fraction Discriminator of model CF 8000 from EG & G. Finally a Fan In/Out-unit from Phillips Scientific was utilized.

3.3 Procedure

A Barium-Fluoride-detector (BaF) was placed behind blocks of lead together with the radioactive sample. The BaF-detector measured the start time while the larger NE213 detector measured the stop time.

The measurements were kept quite simple. The start signal received from the BaF-detector opened a time window of 200 ns. If something was detected with the NE213-detector during that time window, a coincidence had occurred. The Time-to-Amplitude-Converter transformed the flight time into electrical pulses that were digitized and recorded with the transient recorder together with the pulse shape.

When a coincidence was detected, one channel on the TR card recorded time of the pulse and a second channel recorded the actual pulse shape from the liquid scintillator.

A Time-to-Pulse-height-converter transformed the time difference to an electrical pulse so it could be measured and stored with the TR card.

The count rate was low, around 1-5 coincidences each second, depending on the amount of lead blocks placed between the detectors. Investigations on the effects of detector shielding can be found in [9].

The gammas could clearly be distinguished from the neutrons because of the difference in flight time and this was used to verify the results from the pulse shape analysis.

4. Pulse Shape Analysis

The shape of the pulse contains useful information and to be able to extract it one must have some form of analysis tool. There are many available methods to chose from, each method with its advantages and drawbacks.

The chosen method should be simple and computationally effective, but avoid getting unnecessary elaborate and complicated. In addition, it should also be robust and easy to modify and alter. A good and general method with lots of possibilities is the optimum.

The idea is to compare the pulse shape separation results with those from the TOF-separation.

4.1 Overview of methods

There are many ways to analyze a pulse and study its shape to separate it from pulses caused by different interactions. Neutron emission is often accompanied by gamma rays and the pulses looks quite similar at the first glance. Various methods of separating the neutrons from the gammas have been developed.

The NE213 detector is especially useful for pulse shape analysis (PSA) due to its fast response time and the difference between prompt and delayed fluorescence. Many methods focus on the difference between the light emitted in the pulse peak and the tail. It is both a simple and useful method.

In many organic scintillators the observed scintillation light comes from prompt fluorescence. The long-lived component corresponds to delayed fluorescence. The total light yield curve can in a simple model often be represented by the sum of two exponentials, corresponding to the fast and the slow part of the pulse. More complex models use three or more components.

The fast pulse is an exponential decay with a lifetime of a few nanoseconds, while the slow component has a typical length of several hundred nanoseconds. Most of the light is produced in the fast part and the long-lived tail is quite unimportant except for one thing. It can be used to identify the incoming radiation since the fraction of light that appears in the slow component is dependant on the nature of the exciting particle.

It is therefore possible to use this dependence to differentiate between different particles that deposited the same amount of energy in the detector. This is a common method to eliminate gamma-ray-induced events when organic scintillators are used as neutron detectors.

Other methods use Laplace-transforms or similar transforms to analyze the pulse shape to find differences between gammas and neutrons. The transform methods are quite advanced and complicated. It was also very hard to find detailed information about exactly the transforms were used, but often some kind of mathematical damping theorem with comparison of the corresponding damping

constants was utilized. They seemed to be a bit too advanced and time consuming to try and together with the lack of detailed information they were chosen to be omitted from further investigation.

It is also possible to identify average typical gamma and neutron pulse shapes and estimate the probability for an unknown pulse to be either gamma or neutron induced [10].

Another way of separating the particles is to study different time properties. Time over threshold, rise time or such [11]. Due to the limitations in time resolution of the equipment this method was discarded.

The method that was chosen was based on studying the peak and tail of the pulse and utilizing the difference in the tail to separate the gammas from the neutrons. This means utilizing the difference in the delayed fluorescence by studying the integrated amplitudes for different gates in the digitized pulse.

4.2 Analysis program

A program for handling data and analyzing the pulses was written in the programming language Python. Data from the measurements were stored as binary data of the format UInt8[2]. The length of a pulse was 256, 512 or 1024 bytes depending on the wanted pulse length. The 8-bit resolution gave a dynamic range of 0 to 255.

Storing the data as binaries was a very effective way to contain large amount of data with the use of little disk space. The programs contains of one main programs for displaying the data and handling user input and a package of support functions.

The program uses the package Numarray for effective handling of large arrays. Matplotlib is a package specialized for making beautiful 2D-graphics and was chosen for data displaying. Pylab, a Python implementation of MATLAB, was also used for some data processing.

The PSA-program is capable of processing a data file and separating the gammas and neutrons using input-parameters set by the user. Important variables belonging to each pulse are calculated and functions for saving data to file are available. Functions for displaying the data have also been created. Flawed pulses are stored so they can be re-examined for pile-up identification.

The TOF-program processes two data files, one for flight-times and one containing the pulse shapes. Gammas and neutrons are separated both by flight-time and by pulse shape for creating a good comparison between the methods.

[2] Unsigned 8-bit integers

4.2.1 Pulse shape characteristics:

During the measurements a few strange features were observed. The first was the pulse reflections that came from bad cables and unmatched components. The reflections were usually not a problem since they were delayed and appeared after the pulse had died off. For really big pulses they could be a problem since the reflection appeared in the tail of the pulse before it had completely decayed. Using extra long cables partially solved the problem with the pulse reflections. Figure 13 shows a typical pulse with a delayed pulse reflection.

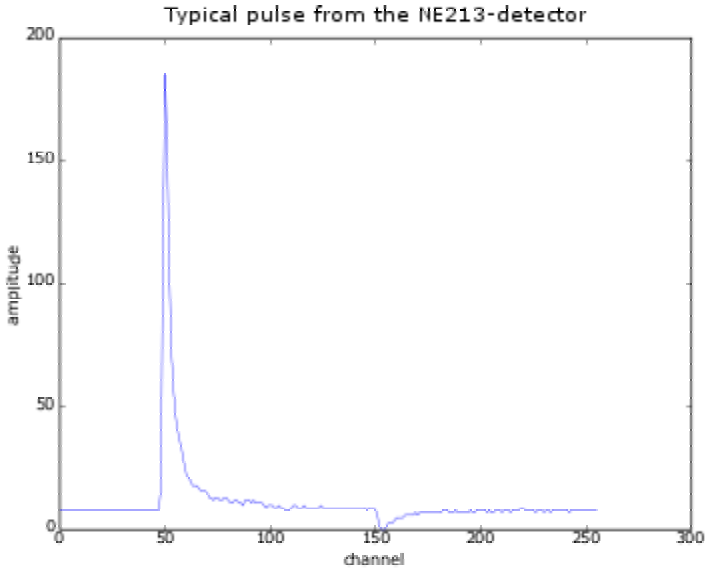

Figure 13: A typical pulse shape obtained from the NE213-detector. The pulse reflection can be seen around channel 150.

Since the transient recorder card only could handle pulses in the range –1 to 0 Volts, it truncated all pulses outside the range. Thus pulses that were truncated because of this were discarded from analysis. Figure 14 displays a typical truncated pulse.

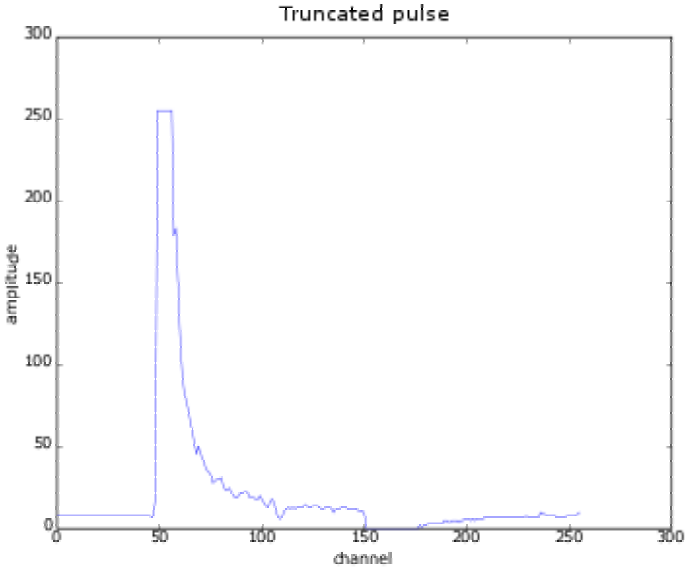

Figure 14: A truncated pulse with a big pulse reflection around channel 150.

Some strange “wiggly” pulses were also seen. They were even more rare than pile-up events and originated from strange software interactions where the wrong data block was grabbed by the data program. Instead of taking the correct pulse shape data, the time stamps were fetched instead, which resulted in the flawed pulses.

In 200 000 pulses, around hundred pulses at most could turn up to be wigglers so they had not any major impact on the measurements and could easily be found and discarded from analysis. Figure 15 shows a wiggler.

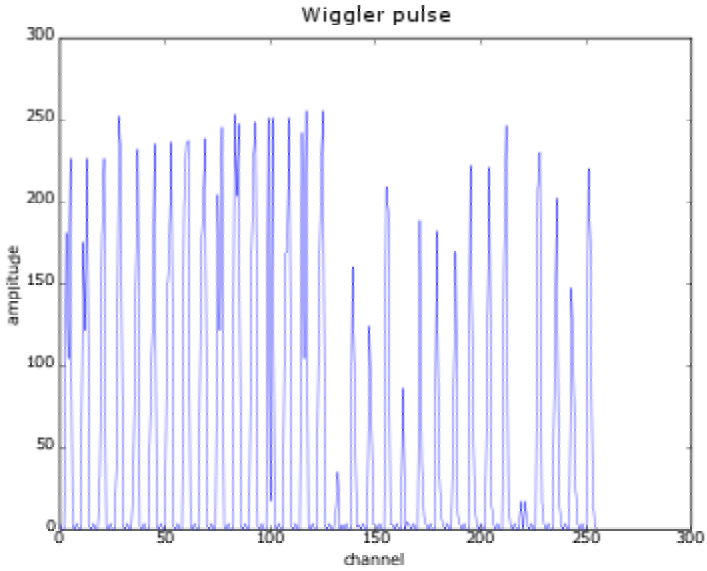

Figure 15: A typical wiggler-pulse

Another problem was pile-up effects. Sometimes two particles hit the detector at nearly the same time and made two pulses appear close to each other within a number of nanoseconds. This can be seen in figure 16. These pile-up events were quite rare with low count rates but increased with increasing count rate. These pile-up events were identified and normally discarded from the further analysis. A great advantage of using digitization of pulses is that post-experiment data processing can be used to treat the pile-up event and extract data from them instead of just discarding them.

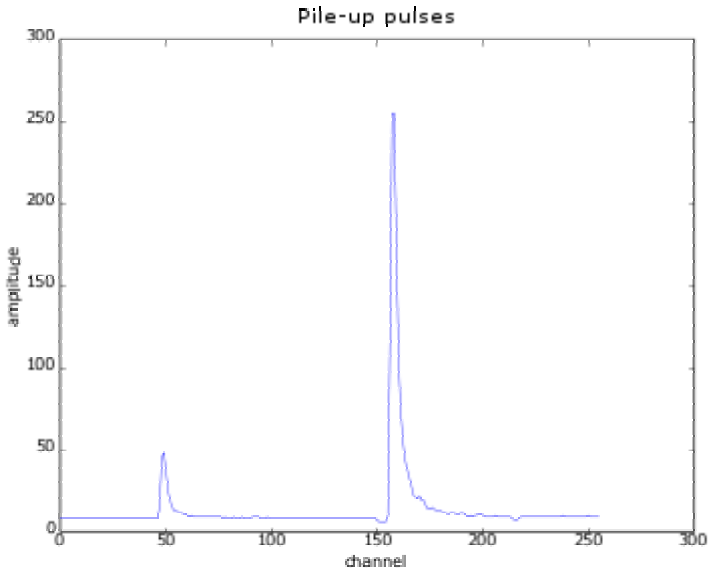

Figure 16: A pile-up event consisting of two pulses.

For each pulse three important points, which marked the area of integration, were defined. From these points and the integrated amplitude between them more variables could be derived. The start point, t_1, was the channel where the pulse started to rise. The intermediate point, t_i, marked where the tail began and the end point, t_2, showed where the pulse ended.

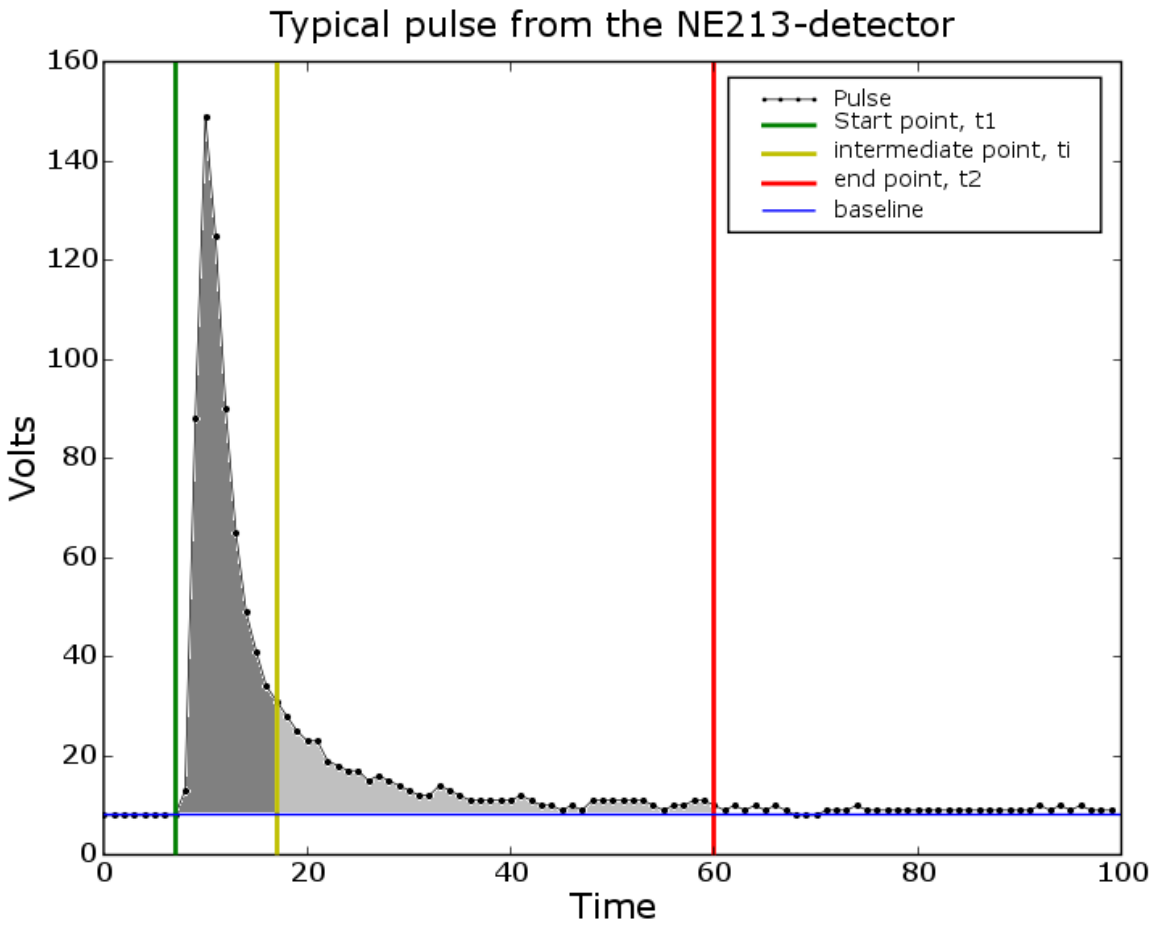

Figure 17: A pulse with the important properties marked. The dark grey area is the peak and the light grey area is the tail.

The integrated amplitude corresponds to the total charge contained in a region. The different nature of the interacting particles will give rise to a difference in the contained charge for gammas and neutrons.

By integrating the amplitude between t_1 and t_i (the dark grey area in figure 17 or figure 18), one obtains the total charge contained in the peak area, called shortgate or I_1. It also has information about the size of the prompt fluorescence.

Integration between t_i and t_2 (the light grey area in figure 17 or figure 18) gives the charge contained in the tail region and information about the size of the delayed fluorescence. From now on this integral is called tail or I_2.

From the integrals I_1 and I_2 one could derive more variables that could be utilized for separation of gammas and neutrons.

The total charge contained in the pulse is the integral from t_1 to t_2 (the sum of the two grey areas in figure 17) and is called longgate or I_{tot}.

By normalizing the longgate (I_{tot}) with the length of the pulse in channels, one obtains the pulse height, which is a measure of the amount of energy contained in the pulse.

The slow/fast constant were defined as the quotient between tail and shortgate (I_2/I_1) and was a measure of how large the tail was compared to the peak region. It is simply the quotient between the slow (delayed fluorescence) light and the fast (prompt fluorescence) light.

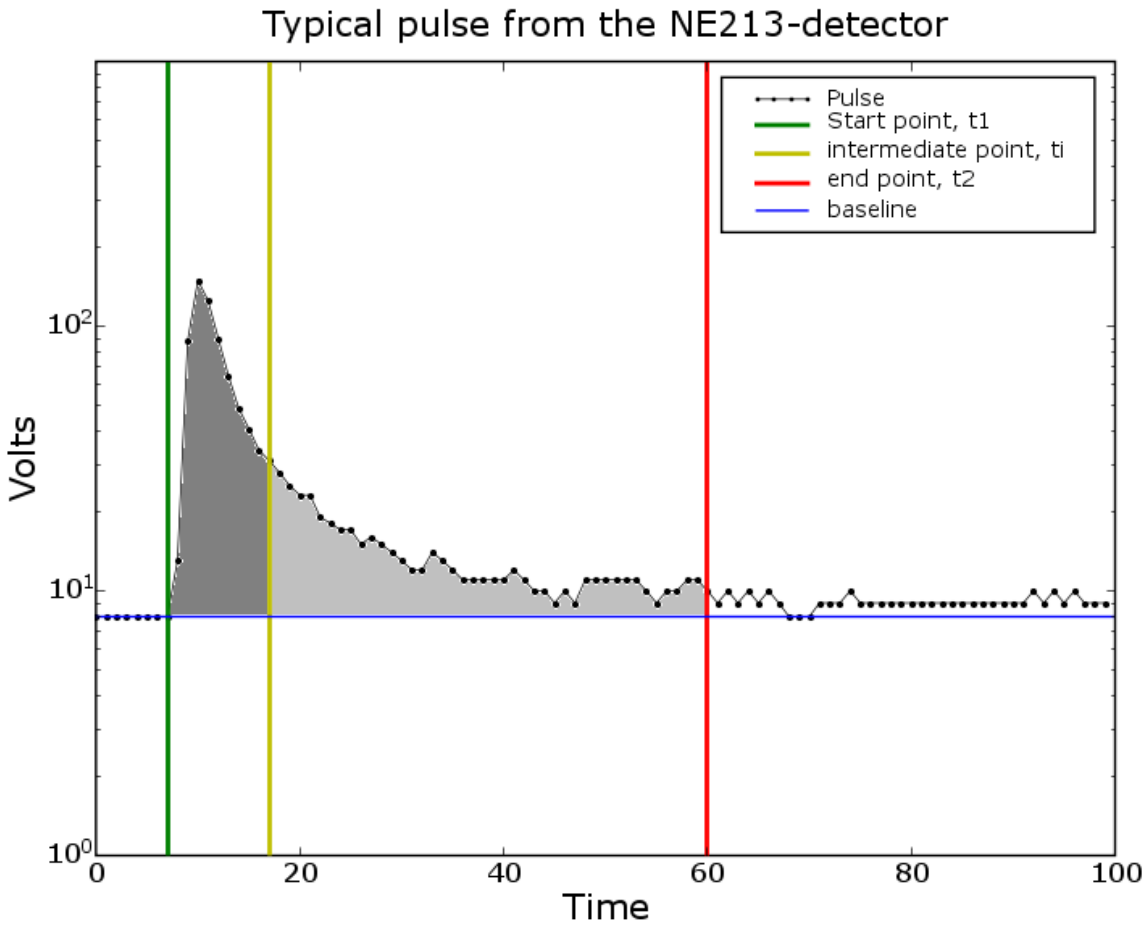

Figure 18: Same data as in figure 17, but in lin-log display.

4.2.3 Quality of the separation and displacement

Some kind of measure for the quality of separation is necessary for studying the efficiency of the separation and how the results vary when the gates are displaced. By making a histogram of the size of the tail one got two peaks, one for small tails and one for large tails corresponding to gammas and neutrons. Gaussians were fitted to these peaks since they looked very gaussian. A figure of merit (FOM) for the separation was defined as the following:

$$\text{FOM} = \text{separation of the peaks} / (2\sigma_{\text{gamma}} + 2\sigma_{\text{neutron}}) \qquad (4.1)$$

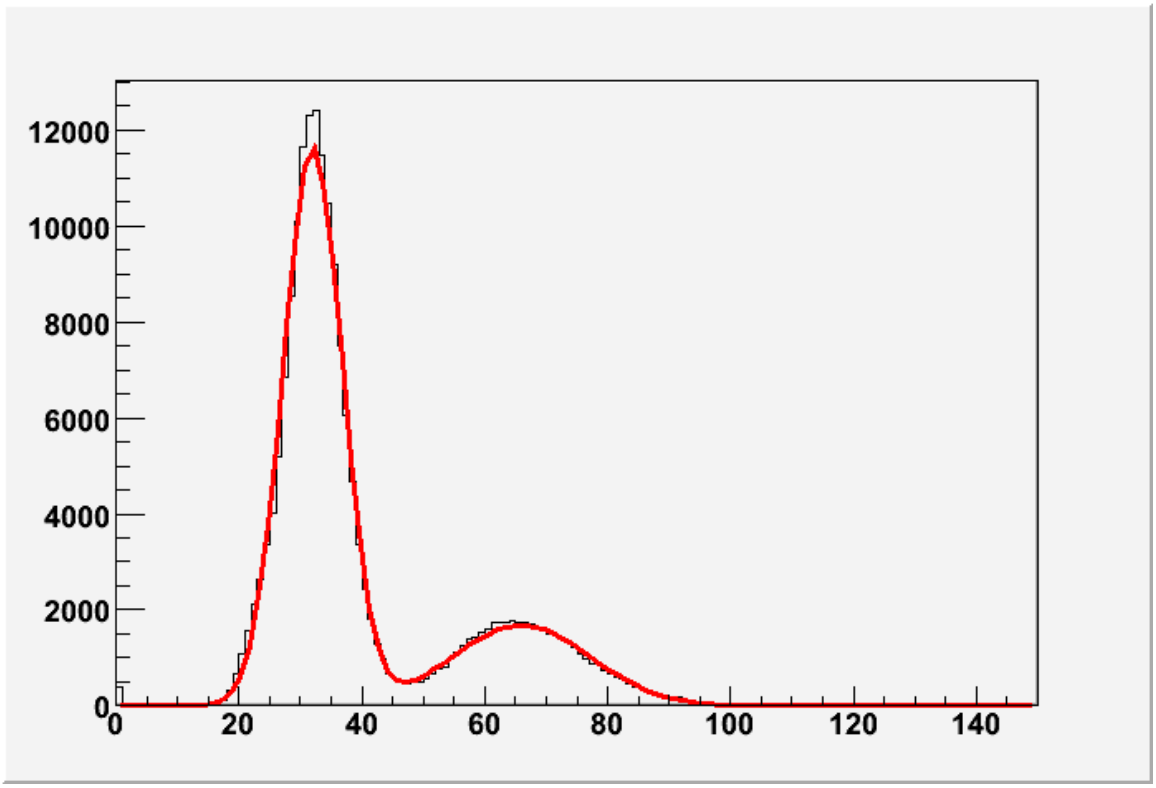

Figure 19: Histogram of the tail. The large and narrow gamma peak is clearly separated from the smaller neutron peak. The figure-of-merit is 1,13.

Data together with two fitted Gaussians can be seen in figure 19. A FOM-value above 1 showed an excellent separation with very little overlap between the gammas and the neutrons. For numbers around 0.5 the two peaks were still separated but a significant amount of overlap between gammas and neutrons could occur, especially at lower energies.

Displacement: The sensitivity of the gates was investigated by shifting the integration points. Starting early before the actual pulse started had little effect compared to starting late and thus missing a large part of the prompt fluorescence. Starting 2 channels to late could ruin everything while you could start 5 channels early and still get a reasonable separation. See figure 20 and 21 for examples of displacement of the gates.

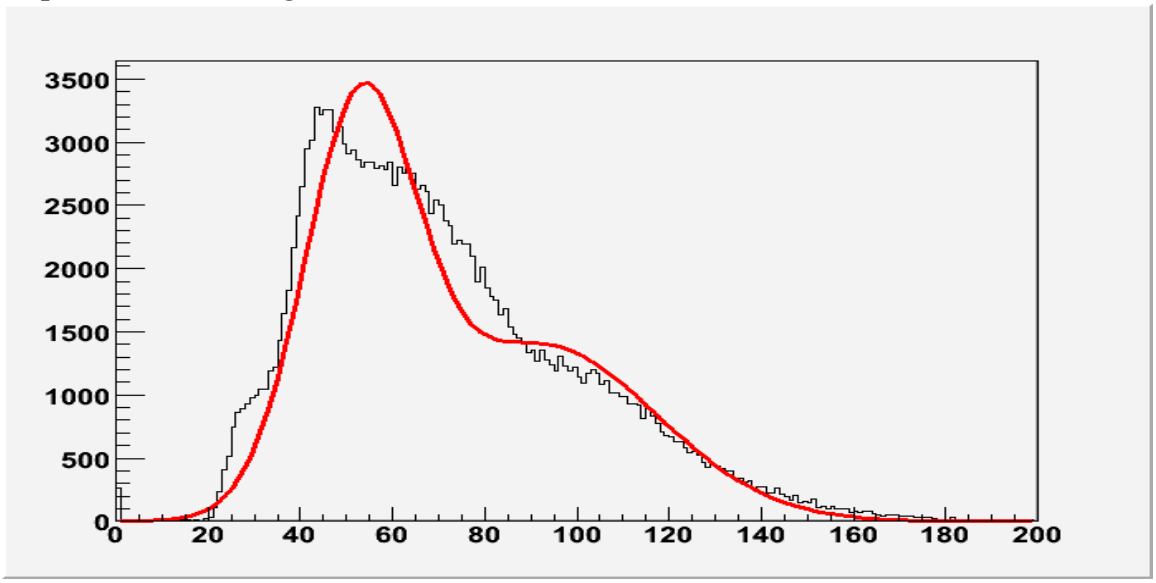

Figure 20: Same data as figure 19 but the gates have been displaced 5 channels earlier. FOM = 0,54

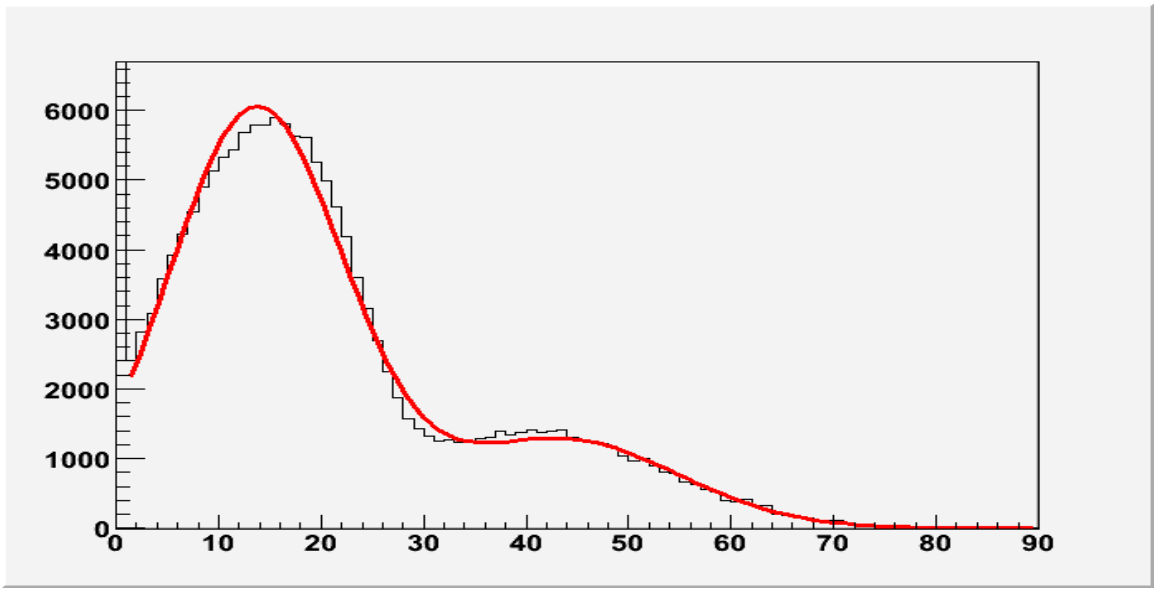

Figure 21: Same data as figure 19 but the gates have been displaced 2 channels later. FOM = 0,78

5. Results

The results from the analysis of the old data and the new measurements showed that it was possible to achieve a good separation of gammas and neutrons with a relatively simple method. The results were also confirmed by comparing them with a TOF-separation.

Energy calibration of the detector was made from Na-22 spectra. For particles with energy of around 100 keV and above it is possible to achieve a good separation, at lower energies than 100 keV a separation can still be achieved but sometimes it becomes quite blurry.

5.1 TOF-results

The results obtained the flight times gave a good separation. The flight time difference for gammas and neutrons made it possible to clearly distinguish between them and thus achieve a good separation that could be used for validation of the PSA-results. By just looking at the flight times one achieved two peaks corresponding to gammas and neutrons. Gammas were much faster than the neutrons and while the slower neutrons had a wider peak because of their different velocities. The results can be seen in figure 22 and 23.

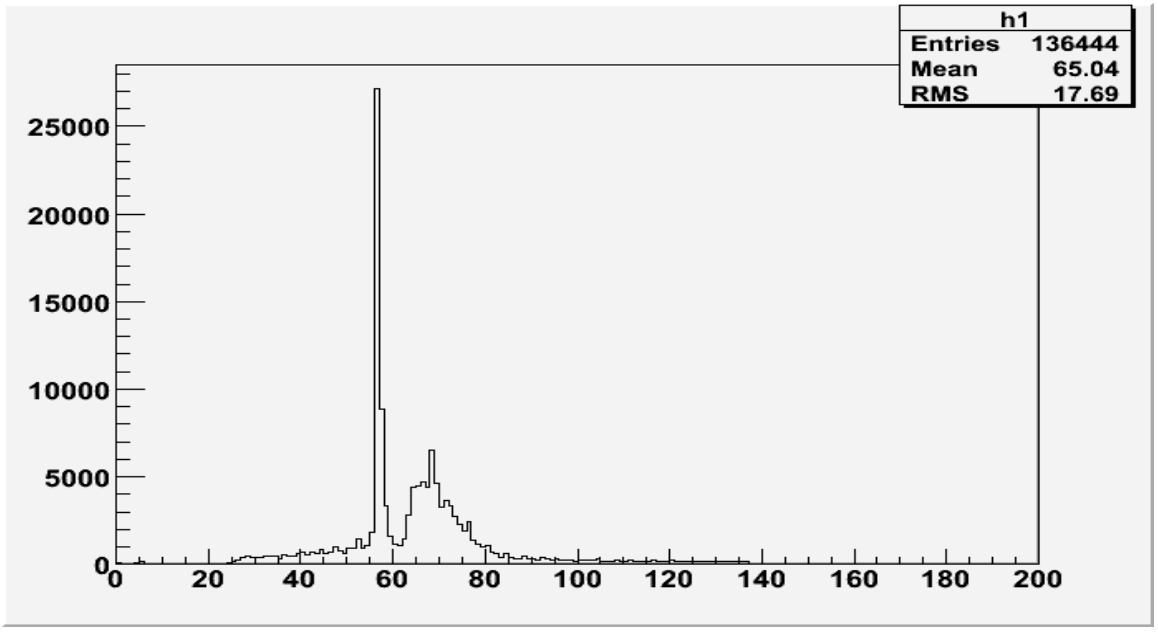

Figure 22: TOF-spectra from the experiment. The first peak corresponds to the gammas while the wider bump corresponds to the neutrons.

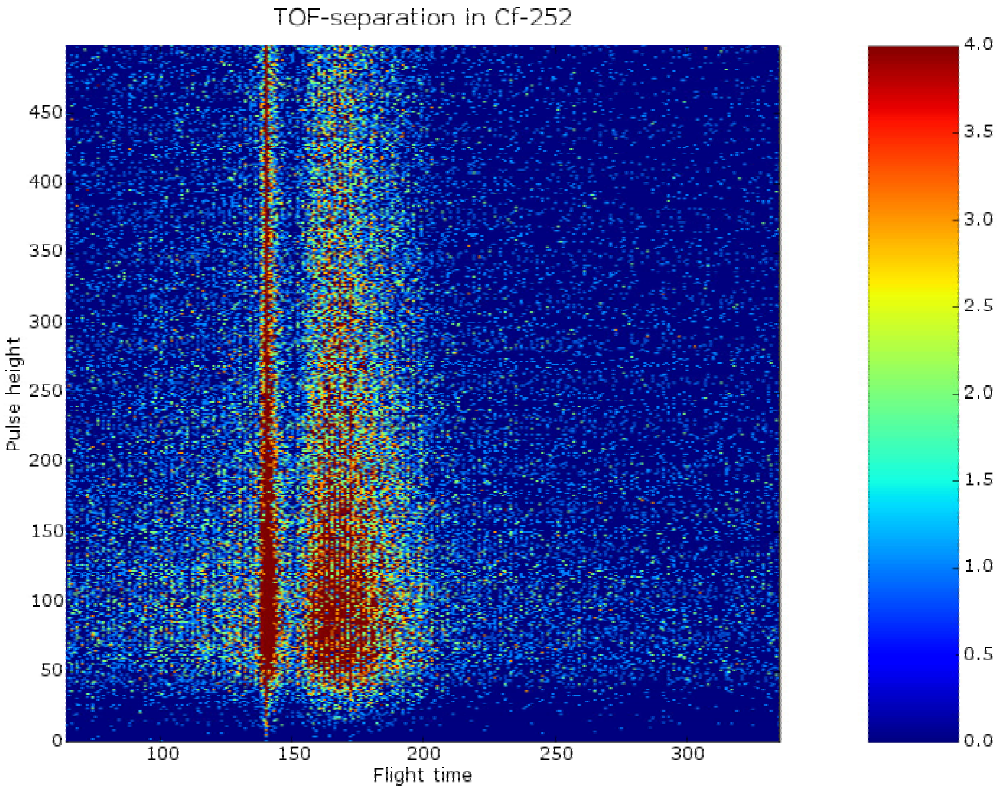

Figure 23: Separation achieved from the time-of-flight measurements. The dataset is approximately 130 000 pulses with around 50% gammas and 50% neutrons. The z-axis is strongly suppressed and can go far higher than 4. Gammas are found to the left and neutrons to the right

5.2 PSA results

The separation is very sensitive to the placement of the gates. Setting the gates right will produce a good separation while misplacement by only a few channels can completely ruin the separation. Therefore, it was important to set the gates right and a large amount of time was spent on investigating different methods of setting them. The gate-setting algorithm was the single most important factor for the quality of the separation.

5.2.1 Setting of gates

The first approach was to use constant gates. This means integrating all pulses from the same time positions. The only advantage of this method was that it was very quick. The results achieved were often poor, although a good separation could sometimes be achieved for a limited data set. A set of gates that worked for a certain dataset did not work for another. The best gate settings had to be found empirically. The quality of the separation was very dependent on the chosen gates. The results can be seen in figure 24.

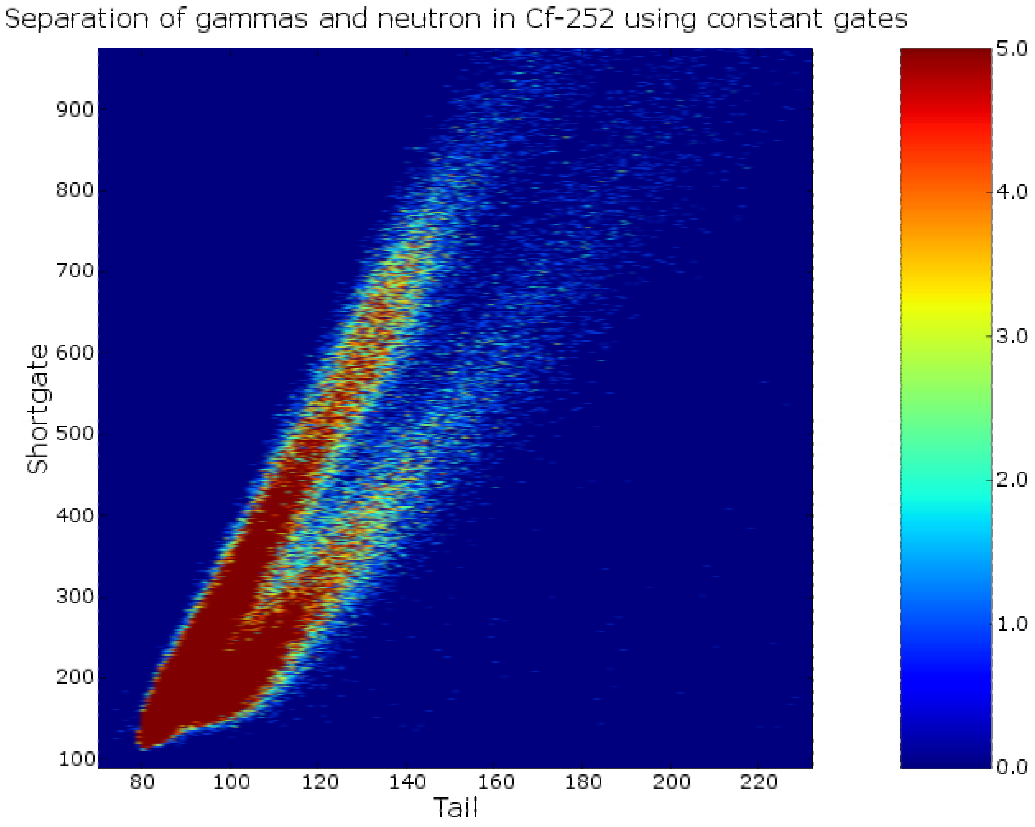

Figure 24: Separation of gammas and neutron. The gammas are found in the upper branch and the neutrons in the lower branch. The z-axis is strongly suppressed and can go far higher than 5.

The second approach was to study each pulse individually and set the gates depending more on the pulse shape. By trying and fit the start point a bit better a better separation could be obtained. Since the pulses rise to the peak value very quick it seemed useful to locate the maxima and set the start point slight before the peak. This resulted in a slightly better separation but a loss in computational speed. Locating the maxima for each individual pulse was time consuming but the improved results justified the longer time. Locating the maxima and adding a number of channels to get the shortpoint and the startpoint improved the results compared to using constant gates.

This method could be further improved by adjusting the length of the shortgate. A very big pulse would have a longer shortgate than a small one and by taking the amplitude into account it was possible to improve separation more. The improved results can be viewed in figure 25.

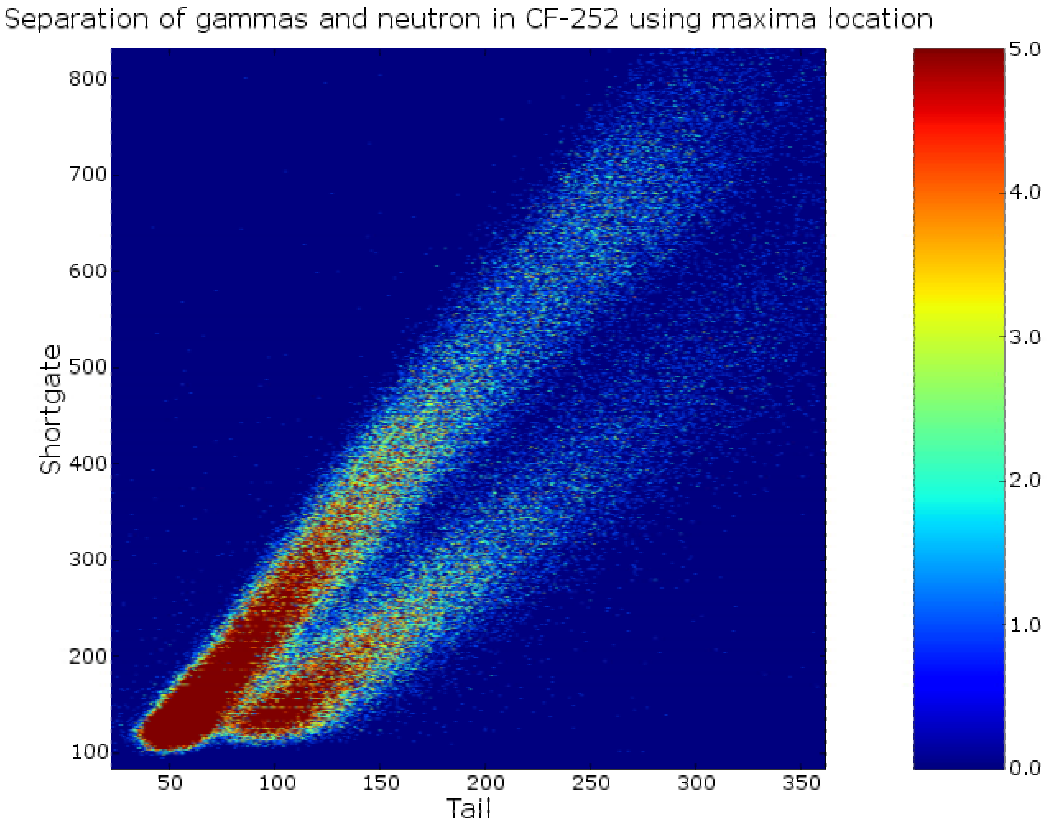

Figure 25: Separation of gammas and neutrons by locating the maxima as startpoint and adding a number of channels to obtain the intermediate point and the end point. The z-axis is suppressed and can go much higher than 5.

A third approach was to use the peak amplitude to determine the length of the shortgate. Locating the startpoint by using the peak amplitude and then setting the shortpoint by adding a number of channels determined by the maximal amplitude and finally terminating the tail before the pulse reflections started to appear. This gave a better separation and also produced some other useful properties.

This is a beautiful way of displaying the data as it opened for several possibilities. Projection on the x-axis gave a way of measuring the quality of the separation. A single constant value can be used to mark the divining line between the gammas and neutrons as well. The simplicity of using this plot made it a personal favorite. The results can be seen in figure 26.

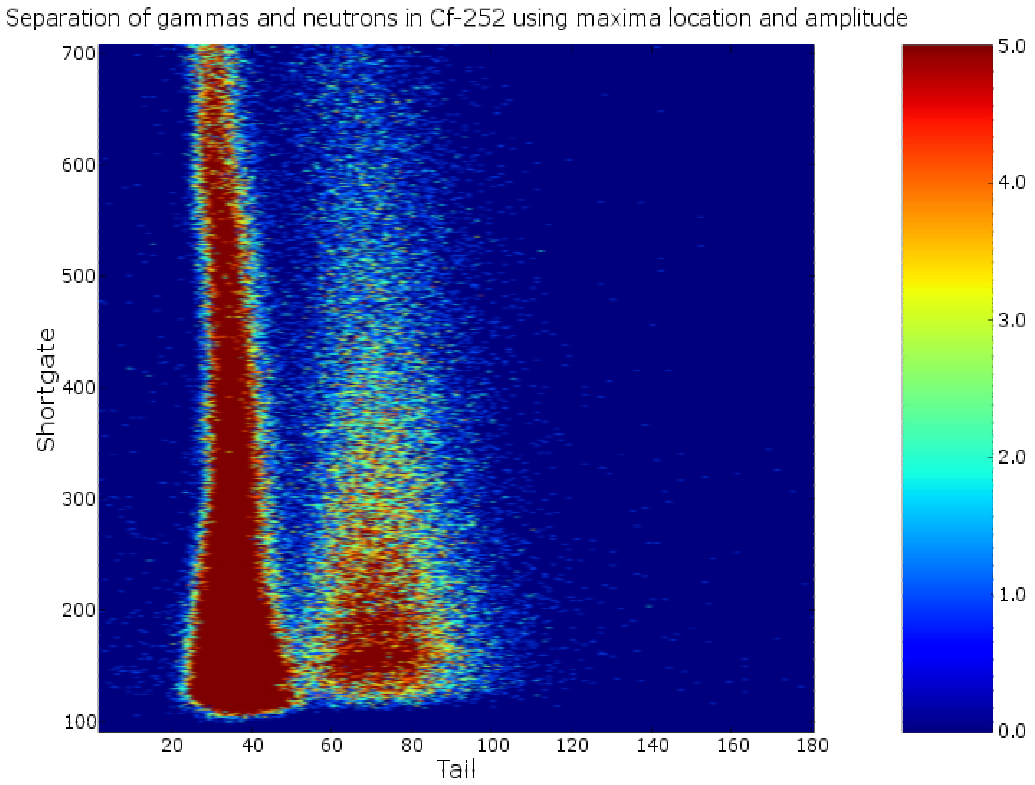

Figure 26: Separation in Cf-252 by using the maximal amplitude for gating. The slopes of the lines have now almost disappeared since both tail and shortgate are functions of the maximal amplitude. The slight bending of the lines comes from pulse reflections that interfere with the tail. The z-axis is suppressed and can actually go much higher than 5 in red areas.

The improved algorithm for setting the gates could also be used for creating an easy way of measuring the quality of the separation. By projecting down on the x-axis one could fit two Gaussians and define a figure of merit.

A fourth way is to plot the integrated amplitude between startpoint and shortpoint, called shortgate, against the integrated amplitude from startpoint to longpoint, called longgate.

This is a direct and easy way of separating them. Despite it is quite useful and one can easily fit a line between the gamma line and the neutron line to act as divider. This is a pretty straightforward way of displaying the difference and can be seen in figure 27.

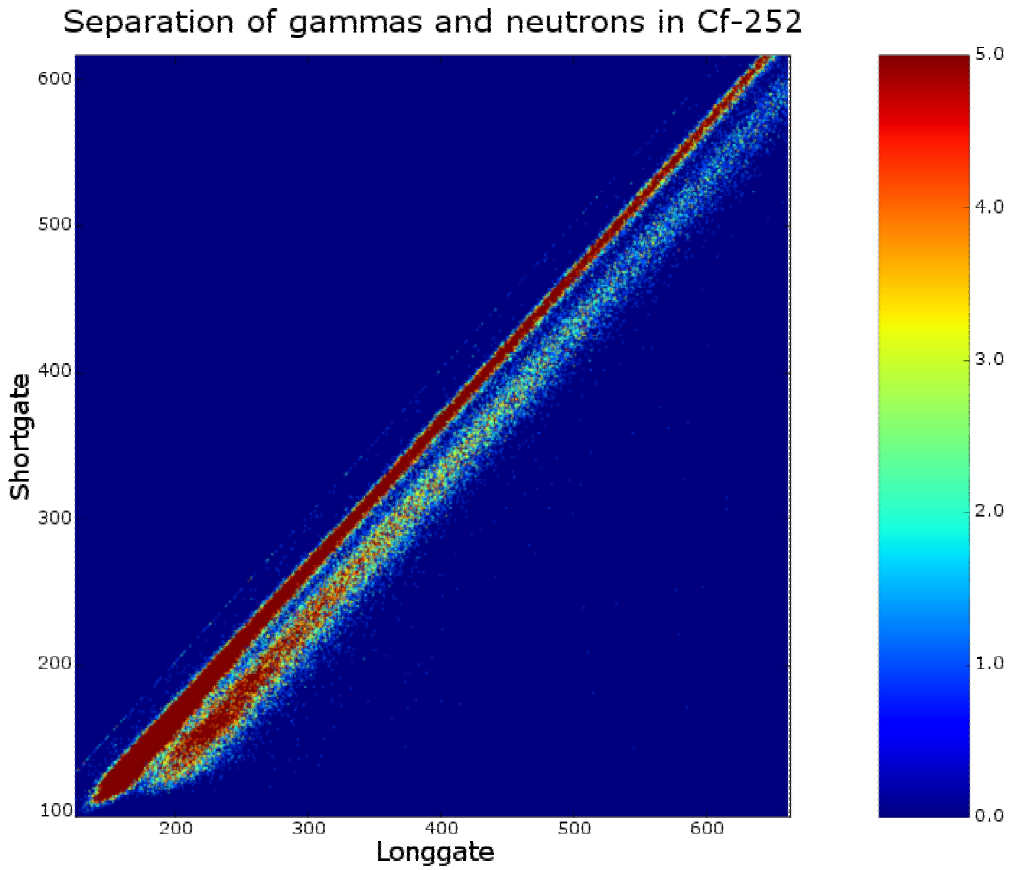

Figure 27: Shortgate vs longgate. The gammas can be found in the upper line and the neutrons in the lower. The z-axis is strongly suppressed and can go far higher than 5.

The fifth approach to displaying the results is a plot of the quotient between the slow light and the fast light against the pulse height. This was a quite nice way of displaying the difference, especially at certain energy. When it comes to smaller energies this way of plotting gives the best results. At 800 keV_{ee} the quotient would be 0,12 for gammas and 0,46 for neutrons according to [12]. This is potentially the plot, which gives the greatest separation, but the drawback is that the areas of interest have a more complicated shape than the other plots. This can be seen in figure 28.

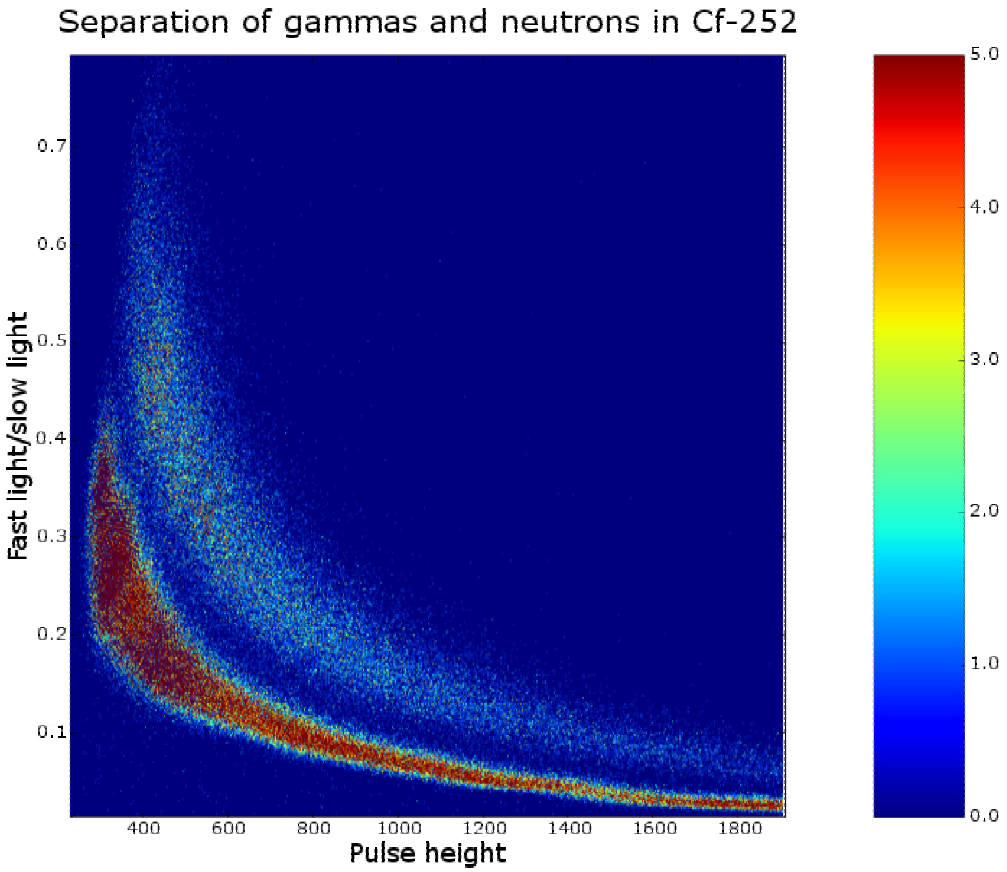

Figure 28: Slow/fast light vs pulse height. Gammas are found in the lower structure and neutrons in the upper. The z-axis is suppressed and can go much higher than 3.

By studying the neutrons found in the neutron area and the gammas from the gamma area one could also make the following studies of the pulse heights. Theoretically the pulse heights of the neutrons are exponentially distributed and this was also found to be true in the measured pulse heights. This match between measurements and theory was taken as an indication of the correctness of the separation. The separated pulse height histograms of neutrons and gammas can be seen in figure 29 and 30.

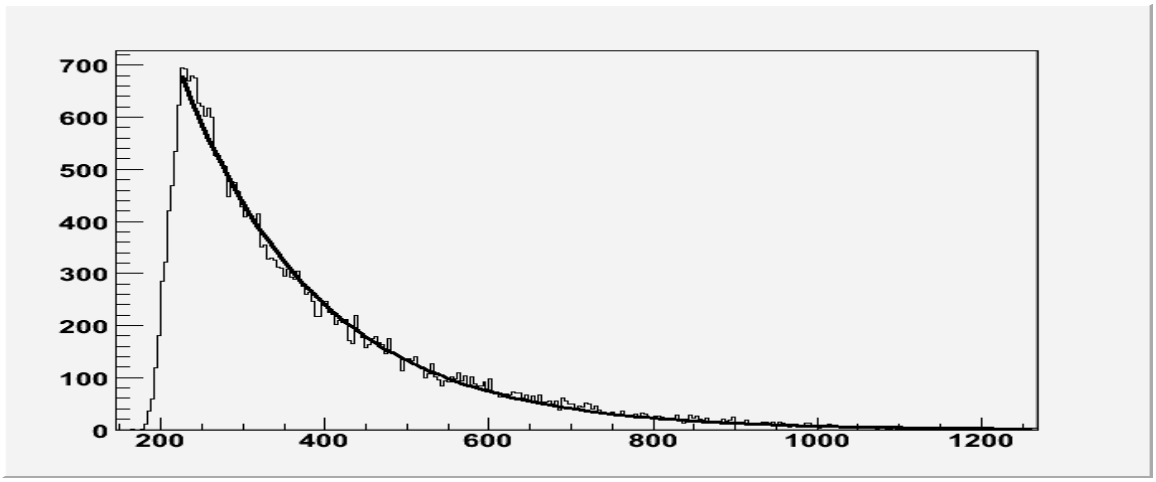

Figure 29: Pulse heights of the neutrons together with a fitted exponential

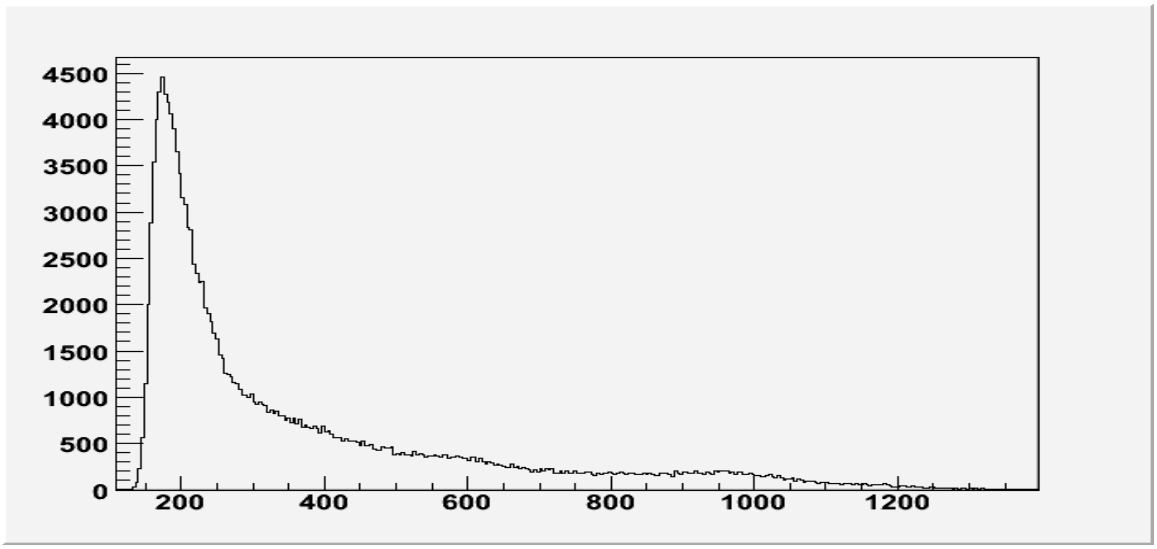

Figure 30: Pulse height histogram for the gammas

5.3 Comparison between PSA and TOF

The comparison between the results achieved in the time-of-flight separation and the results from the pulse shape separation indicated a good level of similarity. Every flight time had a corresponding pulse shape. By doing a PSA-separation and then plotting the flight times corresponding to the pulses one could se if the gamma pulses had gamma flight times and so on.

One could also separate the pulses solely depending on the flight times and then set suitable gates on corresponding pulse shapes to see if the gamma flight times corresponded to gamma pulse shapes. The results can be seen in figure 31 and 32.

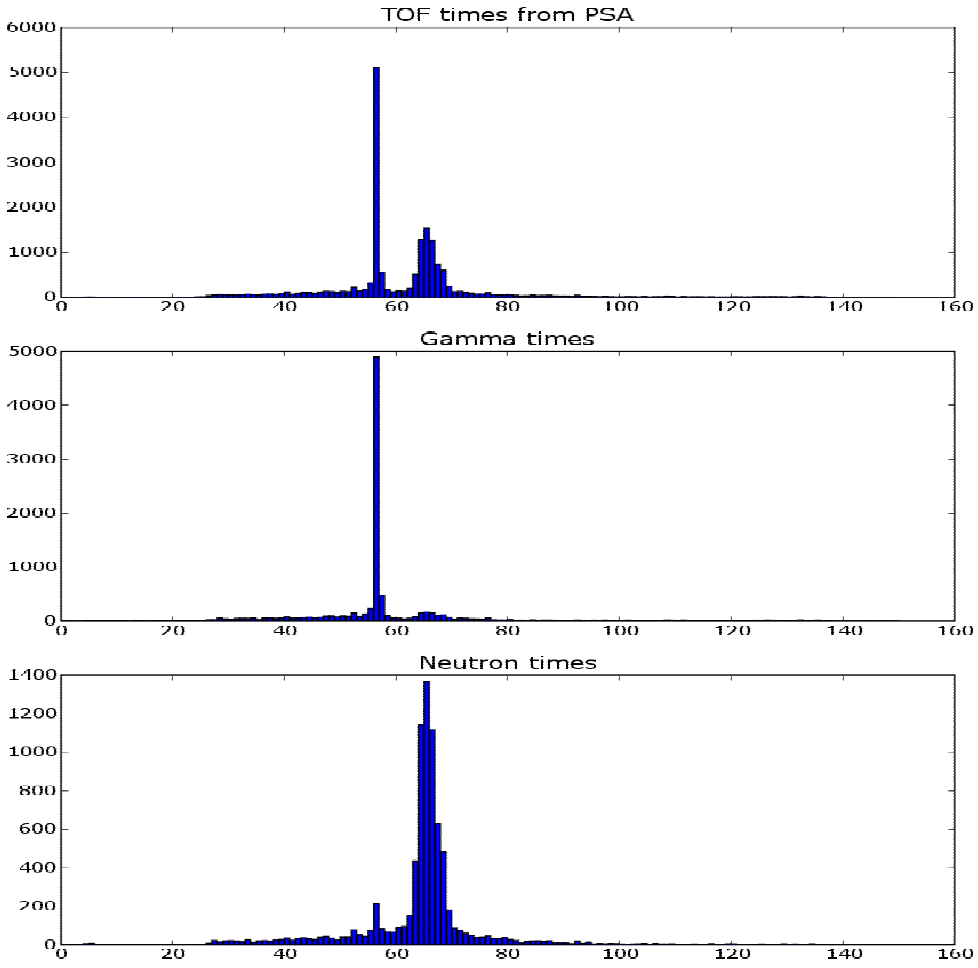

Figure 31: PSA-separation of the pulses and the corresponding flight times. The gamma pulses have typical gamma flight times and the neutrons have neutron flight times. Only a small number of pulses had wrong flight times

The results achieved from PSA and TOF was very similar and the small differences well within the error margins. The correspondence is taken as an indication of the correctness of the PSA-method.

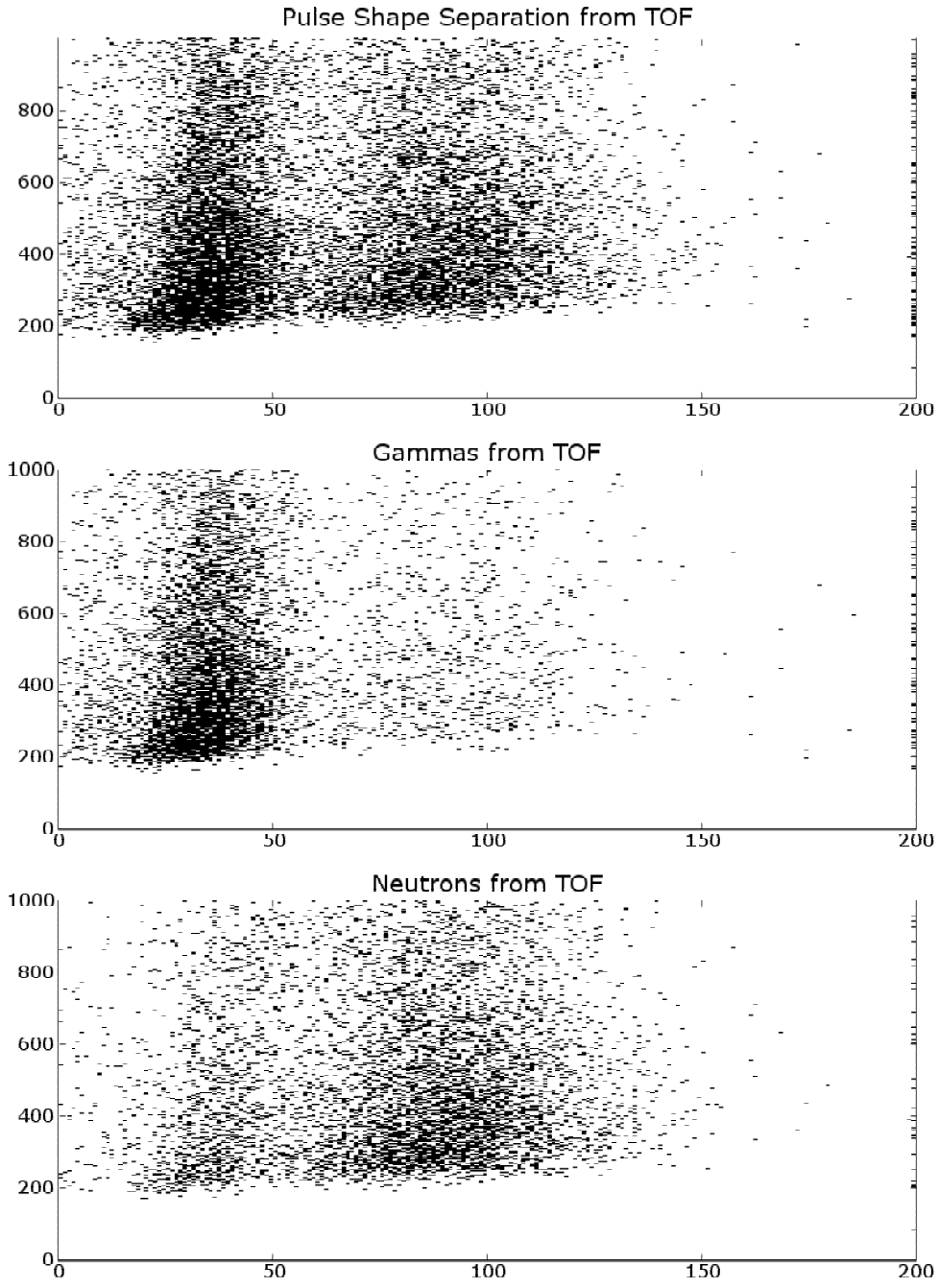

Figure 32: Shortgate vs tail-plots of gammas and neutrons separated by flight times. The gamma flight times also produces gamma pulse shapes while the neutron flight times results in neutron pulse shapes.

6. Conclusion

The results from this thesis show that it is possible to achieve a good separation of gammas and neutrons with a NE213-detector using pulse shape analysis. The results were also confirmed by the TOF-measurements. At low energies the separation deteriorates as expected. At neutron energies of interest down to 0.5 MeV the separation is good. This means that NE213-detection with pulse shape analysis is suitable for fusion applications like neutron cameras and similar instruments.

Some limiting factors and problems were found. One problem was the voltage cut-off from the transient recorder card. Since all pulses smaller than –1 V became truncated and had to be discarded with a loss of valuable data. If one were going to study neutrons with higher energies, it would be useful to be able to handle larger pulses. A larger voltage range of the transient recorder is thus desirable.

The greatest problem was the small pulses, since the difference between gammas and neutrons is less clear. Sometimes the small pulses consisted of a peak without a tail, since the card could not resolve the tail from baseline or arise because the tail had fallen back to baseline before the next data point was taken.

The sampling rate of the card was 200 MHz and that gave a time resolution of 5 ns. For small pulses the time resolution was a limiting factor since 5 ns meant that the data points were taken far to infrequently to catch the entire structure of the pulse. Using sampling rates in the GHz-regime would improve the ability to use small pulses and would probably generate a better overall result.

The 8-bit amplitude resolution is enough for obtaining an acceptable separation, but better resolution would improve the results. For instance, the tail of a small pulse could be better resolved from baseline noise.

Therefore, improvement in both the resolution and the sampling rate is desirable. Better resolution is most desirable, since it would have greatest impact on small pulses.

To further investigate the possibility of pulse shape analysis as a means to separate gammas and neutrons for fusion plasmas, other neutron sources should be studied. Using more high-energy neutrons and perhaps a higher count rate. Preferably sources with higher energy neutrons like Am-Be or neutrons from a neutron generator.

7. Acknowledgements

I would like to thank the following persons who supported me with help, advice and assistance.

Sean Conroy – for giving me the artistic freedom

Anders Hjalmarsson – for all the late Friday nights in the lab

Jan Källne – for all the valuable assistance

MC Hawking – for providing motivation in times of need

8. References

[1] L. Bertalot, B. Esposito – Fast digitizing techniques applied to scintillation detectors,
http://www.bo.infn.it/sminiato/sm04/paper/bertalot.pdf
(Accessed 2006-01-31)

[2] Y. A. Kaschuck, B. Esposito – Fast neutron spectrometry with organic scintillators applied to magnetic fusion experiments, Nuclear Instruments and Methods in Physics Research A, 476 (2002) 511-515.

[3] G. Ranucci – Pulse shape discrimination of liquid scintillators
http://www.lngs.infn.it/lngs_infn/contents/docs/pdf/borexino/…
pulse_shape_discrimination.pdf
(Acessed 2001-01-31)

[4] Glenn F. Knoll – Radiation detection and measurement (Third edition)

[5] Kevin Rudd – Pulse shape discrimination with neutron walls at NCSL
http://www.nscl.msu.edu/~thoennes/personal/theses/rudd.pdf
(Acessed 2001-01-31)

[6] A. Aksoy – Response-Function Measurements of an NE-213 Scintillator Using the 2H(d,n)3He Reaction, Nucl. Instr. & Meth. In Phys. Res. (1994) 486-491

[7] R.A Cecil –Improved predictions of neutrons detection efficiency for hydrocarbon scintillators from 1 MeV to about 300 MeV, Nucl. Instr & Meth. 161 (1979) 439-447

[8] Magnus Hoek – Development and Use of Neutron Scintillator Systems for Fusion Plasma Diagnostics, (Institutionen för reaktorfysik Göteborg) 1992

[9] Ifeta Mesetovic, Therese Nordbeck – Detektionseffektivitet samt effekt av skärmning för neutrondetektorer
http://www.maxlab.lu.se/kfoto/publications/Ex.arbIfetaTherese.pdf
(Accessed 2001-01-31)

[10] S. Marrone, D Cano Ott – Pulse shape analysis of liquid scintillators for neutron studies
http://www.ba.infn.it/~ntof/publications/shape_nim.pdf
(Accessed 2001-01-31)

[11] William L. Bryan, Charles L. Britton – Fast neutron-gamma pulse shape discrimination of liquid scintillation signals for time-correlated measurements
http://www.ornl.gov/~webworks/cppr/y2001/pres/118872.pdf
(Accessed 2001-01-31)

[12] B. Naranjo, J.K. Gimzewski – Observations of nuclear fusion driven by a pyroelectric crystal (supplementary methods), Nature 434 (2005) 1115-1117